Precambrian Research 270 (2015) 124–138

Contents lists available at ScienceDirect

Precambrian Research

journal homepage: www.elsevier.com/locate/precamres

2.24 Ga mafic dykes from Taihua Complex, southern Trans-North China Orogen, and their tectonic implications

Jinsheng Han[a], Huayong Chen[a], Junming Yao[a,*], Xiaohua Deng[b]

[a] Key Laboratory of Mineralogy and Metallogeny, Guangzhou Institute of Geochemistry, Chinese Academy of Sciences, Guangzhou 510640, China
[b] Beijing Institute of Geology for Mineral Resources, Beijing 100012, China

ARTICLE INFO

Article history:
Received 15 April 2015
Received in revised form 17 August 2015
Accepted 4 September 2015
Available online 11 September 2015

Keywords:
The Zhaiwa mafic dykes
SCLM
Terrigenous sediments
Taihua Complex
North China Craton

ABSTRACT

LA-ICP-MS U–Pb zircon geochronological, geochemical and Sr–Nd isotopic data are presented for the mafic dykes in the Zhaiwa Mo deposit, Taihua Complex to characterize the tectonic setting of the southern Trans-North China Orogen (TNCO). These mafic dykes intruded the Taihua Supergroup and yield a concordant $^{207}Pb/^{206}Pb$ age of 2242 ± 25 Ma. The zircon grains have initial $^{176}Hf/^{177}Hf$ values of 0.281012–0.281194, with negative $\varepsilon Hf(t)$ values ranging from −11.4 to −2.7 and T_{DM} ages ranging 2805–3051 Ma. Whole rock geochemistry shows that the dykes are doleritic and have high Fe contents, which usually possess relatively high density. The $(^{87}Sr/^{86}Sr)_t$ (t = 2242 Ma) values fall into two groups, i.e., 0.705605–0.707058 and 0.725237–0.748725. The $\varepsilon Nd(t)$ values (−6.67 to −3.27, with corresponding T_{DM} ages of 3020–4063 Ma) indicate an enriched mantle source. Geochemical characteristics of the Zhaiwa mafic dykes, including the low TiO_2 (0.94–2.00%) and enriched Sr–Nd isotopes, suggest their derivation from a sub-continental lithospheric mantle (SCLM) source modified by recycled sediments. Simulation calculations imply the absence of garnet in the mantle source, indicating the emplacement of these mafic dykes in an extensional setting, e.g., back-arc rifting. Our work implies the existence of a back arc basin at 2.24 Ga in the southern TNCO and the final collision between the Eastern and Western Blocks of the North China Craton must have happened after 2.24 Ga.

1. Introduction

The North China Craton (NCC), which is the oldest known Craton in China and contains massive Archean to Paleoproterozoic rocks (Liu et al., 1992; Zhao et al., 2003), has been attracting more and more attentions of researchers. Although the tectonic model that the North China Craton was formed by the amalgamation between the Western Eastern Blocks of the NCC along the Trans-North China Orogen (TNCO) has been accepted by most scholars (Fig. 1a; Diwu et al., 2014; Huang et al., 2012; Kusky et al., 2007; Yu et al., 2013; Zhao et al., 2001, 2005), controversies still have been arised as to the formation of the TNCO: (1) some researchers suggested that the final amalgamation resulted from a westward subduction at ~2.5 Ga (later modified to 2.3–2.2 Ga) (Kusky and Li, 2003; Kusky, 2011; Li and Kusky, 2007; Zhai and Liu, 2003); (2) some others proposed a eastward subduction with the final amalgamation at ~1.85 Ga (Zhao et al., 2001, 2003, 2005); (3) the others suggested a westward subduction with two Paleoproterozoic collisions at ~2.1 Ga and ~1.85 Ga, with ~2.1 Ga accounting for the amalgamation of the eastern blocks with the Fuping Block (Faure et al., 2007; Trap et al., 2007, 2012) or between the accreted Lvliang–Hengshan–Wutai–Fuping arc terranes and the Western Block (Wang et al., 2010) and ~1.85 Ga accounting for the main structural, metamorphic and magmatic features of the TNCO (Faure et al., 2007; Trap et al., 2007, 2012; Wang et al., 2010). To resolve these controversies, knowing what happened at 2.2–2.1 Ga is of great importance to constrain the building-up of the TNCO (Faure et al., 2007; Trap et al., 2007; Wang et al., 2010; Zhou et al., 2015).

Indeed, a great deal of works show that 2.2–2.1 Ga geologic events are widespread along the TNCO. Most of these studies are mainly based on granitoids, granitic gneisses, meta-sediments in the Hengshan Complex, Wutai Complex, Fuping Complex, Lvliang Complex and Zanhuang Complex (Fig. 1a; Du et al., 2010, 2012, 2013; Kröner et al., 2005; Liu et al., 2012; Liu et al., 2014a,b; Peng et al., 2012; Zhao et al., 2011). Some limited studies about mafic igneous rocks generated during 2.2–2.1 Ga have also been reported mainly in the Hengshan, Wutai, Huai'an and Fuping complexes (Fig. 1a; Peng et al., 2005, 2012; Wang et al., 2010). A continental rift basin setting contradicts with subduction-related setting regarding the tectonic setting of the TNCO during 2.2–2.1 Ga based

* Corresponding author. Tel.: +86 20 8529 0207.
E-mail address: yaojunming@gig.ac.cn (J. Yao).

http://dx.doi.org/10.1016/j.precamres.2015.09.009
0301-9268/

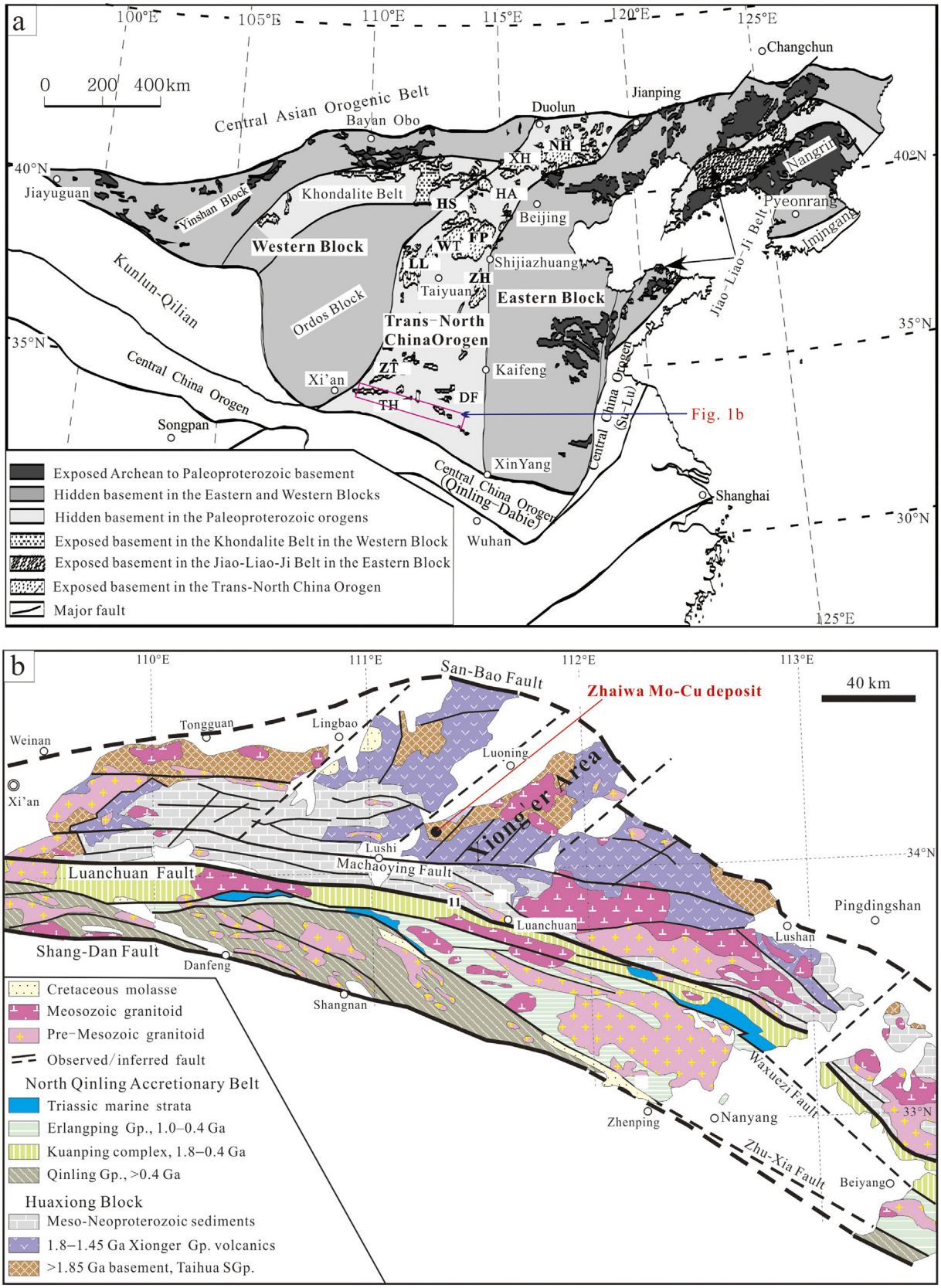

Fig. 1. (a) Tectonic subdivision of the North China Craton (modified after Zhao et al., 2005); Abbreviations for metamorphic complexes: NH, Northern Hebei; XH, Xuanhua; HA, Huai'an; HS, Hengshan; FP, Fuping; WT, Wutai; LL, Lvliang; ZH, Zanhuang; ZT, Zhongtiao; DF, Dengfeng; TH, Taihua. (b) Geological distribution of the Taihua Complex in the southern NCC and the location of the Zhaiwa Mo deposits (after Li et al., 2014).

on the above studies, meanwhile, most of these rocks studied are mainly distributed in the northern part of the TNCO, with studies of contemporary rocks in the southern part of the TNCO rare, which in turn limits our understanding of the tectonic evolution of the TNCO in the Palaeoproterozoic.

Studies on mafic dykes are more useful to constrain the tectonic environment for their short life span, good capacity to preserve their original chemical characteristics and recording information regarding the chemical composition of the mantle and regional tectonic evolution (Ma et al., 2013; Peng et al., 2012; Wei et al., 2014). In this contribution, a detailed study on petrology, geochronology, geochemistry and Sr–Nd–Hf isotopes for the Zhaiwa mafic dykes in the Taihua Complex (in the southern part of the TNCO) are presented for the first time. The results provide clear evidence that the lithospheric mantle was at least locally enriched by recycled crustal sediments during previous subduction-collision processes. Our results help to clarify the petrogenesis and geodynamic setting of the Zhaiwa mafic dykes and shed light on the tectonic evolution of the TNCO combined with previous studies.

2. Geological background

The North China Craton (NCC), which is the oldest known craton in China and contains massive Archean to Paleoproterozoic rocks (Liu et al., 1992; Zhao et al., 2003), is bounded by the Central Asian Orogenic Belt to the north, the Qinling-Dabie Orogenic Belt to the south, the Kunlun-Qilian Orogenic Belt to the west, and the Su–Lu ultrahigh-pressure Metamorphic Belt to the east (Fig. 1a). According to lithological, geochronological, structural and thermobarometric data, the NCC can be divided into distinct Western and Eastern Blocks along the Trans-North China Orogen (TNCO) (Zhao et al., 1998, 2001, 2003, 2005). The Western Block can be further divided into the Yinshan Block in the north and Ordos Block in the south along the Khondalite Belt, which was formed at ~1.95 Ga (Zhao et al., 2005). Meanwhile, the Eastern Block is composed of the Longgang and Langrim Blocks along the Paleoproterozoic Jiao-Liao-Ji Belt, which was formed at ~1.9 Ga (Li and Zhao, 2007).

The TNCO consists of Dengfeng, Fuping, Hengshan, Huai'an, Lvliang, northern Hebei, Taihua, Wutai, Xuanhua, Zanhuang and Zhongtiao complexes, which are predominantly composed of varying proportions of late Archean to Paleoproterozoic basement rocks metamorphosed into greenschist to granulite facies, with Fuping, Hengshan, Huai'an, Taihua, Xuanhua Complexes as high-grade gneiss terrains (according to lithologies and metamorphic grades) and the others as low-grade granite-greenstone belts (Fig. 1a; Zhao et al., 2005, 2007).

The Taihua Complex, a suite of early Precambrian medium-high grade metamorphic rocks composed of a series of graphite-bearing gneisses, biotite gneisses, marbles and banded iron formations, is widely exposed eastward from the Xiaoqinling to the Xiaoshan, Xiong'er, Lushan and Wugang areas in the southern TNCO, extending from Shaanxi and across Henan to Anhui Province (Fig. 1b; Jiang et al., 2011; Zhang et al., 1985).

The Taihua Complex (Supergroup) in the Xiong'er area was subdivided into, from bottom to top, the Caogou (migmititic gneisses), Shibangou (amphibolites), Tieluping (BIF-containing), Longtangou (marble-bearing) and Duangou (khondalite-bearing) Formations (Chen and Fu, 1992). The Caogou Formation is composed of biotite plagioclase gneiss and amphibolite plagioclase gneiss. The Shibangou Formation is the most widespread sequence of the Taihua Complex in the Xiong'ershan area. It covers the Caogou Formation comfortably and consists mainly of amphibolite plagioclase gneiss, amphibolite, biotite plagioclase gneiss, intercalating with some layers of leptynite and marble. The Duangou Formation, which covers the Shibangou Formation uncomfortably, consists mainly of high-grade sillimanite–garnet gneisses, graphite-bearing gneisses, with minor mafic granulites, amphibolites (Zhang and Li, 1998). In the Xiong'er area, the Taihua Complex was covered uncomfortably by the widespread Xiong'er group, a well-preserved non-metamorphosed volcanic sequence, consisting mainly of basaltic andesite, trachyandesite, dacite, rhyolite and volcanic tuff which erupted intermittently over a protracted interval from 1.78 Ga, through 1.76–1.75 Ga and 1.65–1.45 Ga, with the major phase of the volcanism at 1.78 Ga (He et al., 2009; Zhao et al., 2009). Several Mesozoic Yanshanian granitoids had intruded the above lithostratigraphic units.

The Zhaiwa Mo–Cu deposit is hosted by the Taihua Complex in the Xiong'er area and represents the upper domains of a porphyry mineral system developed in a continental arc (Fig. 1b; Deng et al., 2013a,b). Re–Os dating showed that the Zhaiwa deposit formed at ~1.76 Ga (Deng et al., 2013b). Several mafic dykes (we call them the Zhaiwa mafic dykes hereafter) intruded the Taihua Complex (the Shibangou Formation) in the Zhaiwa Mo–Cu deposit (Fig. 2).

3. Sampling and petrography

The Zhaiwa mafic dykes, located in the mine area of the Zhaiwa Mo–Cu deposit, had intruded the Taihua Supergroup (Fig. 2a and b). We try to select six freshest samples and the sample locations are shown in Fig. 2. Petrographic study reveals that the Zhaiwa mafic dykes are locally chloritized and mainly composed of plagioclase and orthopyroxene and minor magnetite. The plagioclase grains are usually large and subhedral to euhedral. The orthopyroxene grains are usually small and anhedral and occur along cracks of plagioclase, show somewhat ophitic texture (Fig. 3c and d). Detailed geological descriptions of the Zhaiwa deposit were given in Deng et al. (2013b).

4. Analytical methods

4.1. Zircon U–Pb dating and trace elements

Zircon grains used for U–Pb dating were separated using standard density and magnetic separation techniques. The grains were then hand-picked under a binocular microscope, mounted in epoxy resin and polished to expose the crystal facies. Internal structure of the zircon grains was examined using cathodoluminescence (CL) before the U–Pb dating.

The U–Pb dating was done by Laser Ablation Inductively Coupled Plasma Mass Spectrometry (LA-ICP-MS) at the State Key Laboratory of Isotope Geochemistry, Guangzhou Institute of Geochemistry, Chinese Academy of Sciences (GIG-CAS). Resolution M-50 laser-ablation system and Agilent 7500a ICP-MS were combined for the experiments. The laser energy was 80 mJ with the frequency as 6 Hz and an ablation spot of 31 μm in diameter. The ablated aerosol was carried to the ICP-MS with He gas. Zircon 91500 was used as the external standard while NIST SRM 610 as the internal standard (Wiedenbeck et al., 1995). Detailed analytical processes were outlined in Yuan et al. (2004). Calculations of zircon isotope ratios and trace elements were performed by ICPMSDataCal 7.0 (Liu et al., 2010). Zircon ages were calculated using Isoplot (Version 3.0; Ludwig, 2003).

4.2. Whole-rock geochemistry

Whole-rock major elemental geochemistry was determined using Rigaku RIX-2000 X-ray fluorescence (XRF) at the Analytical Laboratory of Beijing Research Institute of Uranium Geology (BRIUG), with a precision better than 1–5%. Trace element contents

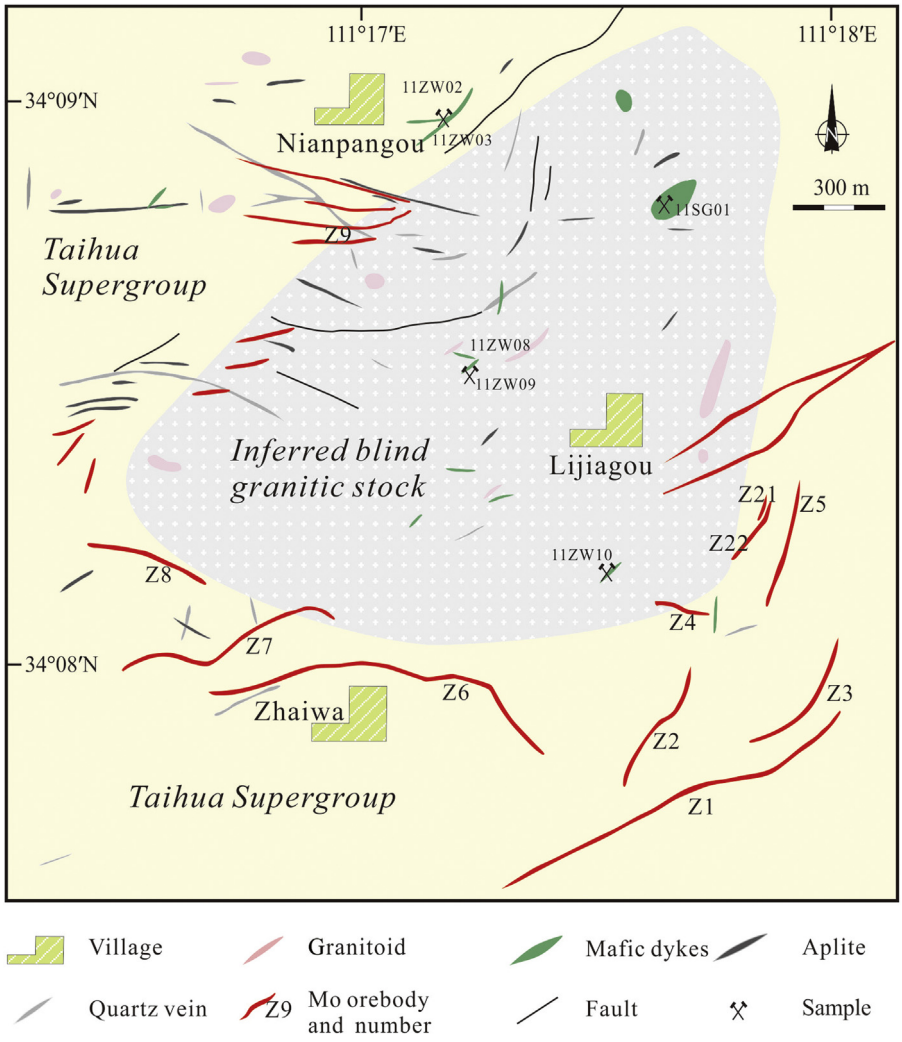

Fig. 2. Geology of the Zhaiwa Mo deposit, showing the position of the mafic dykes (modified after Deng et al., 2013b).

were determined using Perkin-Elmer Sciex ELAN-6000 ICP-MS, with a precision better than 3%.

4.3. Whole-rock Sr–Nd isotopes

Whole-rock Sr and Nd isotopic compositions were determined using a multicollector (MC) Finnigan MAT-261 Thermal Ionization Mass Spectrometry (TIMS) operated in static multicollector mode at the State Key Laboratory of Geological Processes and Mineral Resources, China University of Geosciences (Wuhan). After being powdered with an agate mill to 200 meshes, samples were digested in Teflon bombs with a mixture of concentrated HF and HNO_3 at 190 °C for 48 h. The decomposed samples were then dried on a hot plate and converted into chlorides by adding 2 ml of concentrated HCl. The residue was redissolved in 100 μl $HClO_4$ and concentrated HCl, and subsequently evaporated to dryness. The dried salts were redissolved in 1 ml of dilute HCl and loaded onto columns of AG50W-X8 resin for separation and purification of Sr and rare earth elements (REEs), with the REEs cut finally loaded onto HDEHP columns for separation of Nd by HCl eluants. The measured $^{143}Nd/^{144}Nd$ and $^{87}Sr/^{86}Sr$ ratios were normalized to $^{143}Nd/^{144}Nd = 0.721900$ and $^{87}Sr/^{86}Sr = 0.1194$, respectively. Repeated analyses yielded $^{143}Nd/^{144}Nd$ of 0.511847 ± 3 (2σ, $n = 25$) for the La Jolla standard, $^{143}Nd/^{144}Nd = 0.512637 \pm 3$ (2σ, $n = 2$) for BCR-2, and $^{87}Sr/^{86}Sr = 0.710254 \pm 8$ (2σ, $n = 22$) for SRM NBS-987. Analytical details and analysis of the reference materials were reported in Rudnick et al. (2004).

4.4. Zircon Lu–Hf isotopes

In situ zircon Hf isotope measurements were conducted using LA-ICP-MS with a beam size of 44 μm and laser repetition rate of 8 Hz at the MC-ICPMS laboratory of GIG-CAS. Raw count rates for ^{172}Yb, ^{173}Yb, ^{175}Lu, $^{176}(Hf + Yb + Lu)$, ^{177}Hf, ^{178}Hf, ^{179}Hf, ^{180}Hf and ^{182}W were collected and isobaric interference corrections for ^{176}Lu and ^{176}Yb on ^{176}Hf were precisely determined. ^{176}Lu was calibrated using the ^{175}Lu value and the correction was made to ^{176}Hf. The zircon standards adopted during experimentation were Penglai whose $^{176}Hf/^{177}Hf$ was 0.082906 ± 50. Full details of the analytical methods are provided in Wu et al. (2007). The T_{DM} was calculated using the measured Lu/Hf ratios and present-day $^{176}Hf/^{177}Hf$ ratio of 0.28325 and $^{176}Lu/^{177}Hf$ of 0.0384 of depleted mantle (DM) (Griffin et al., 2000). The average crustal model ages (T_{crust}) were obtained assuming that the protolith from which the host magma of a given zircon was derived from the DM source, and had the $^{176}Lu/^{177}Hf$ of the average continental crust (i.e., 0.0115, Wang et al., 2009).

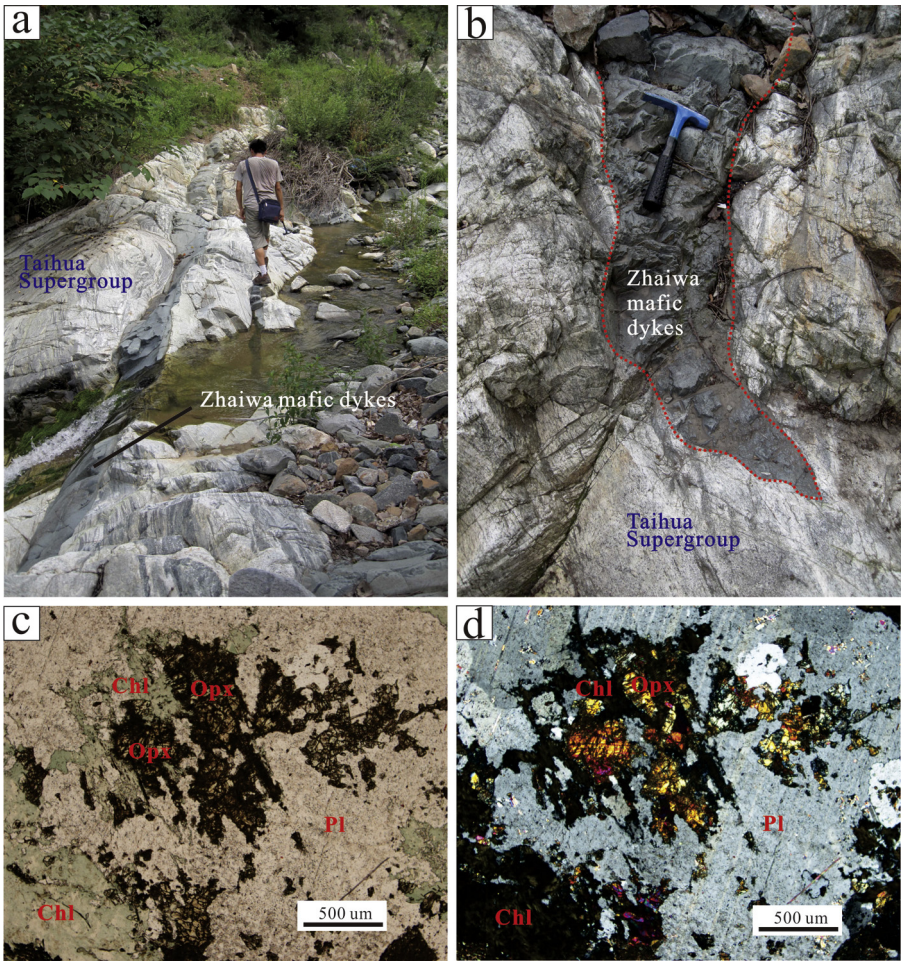

Fig. 3. (a) and (b) Field photographs showing the Zhaiwa mafic dykes intruding the Taihua Supergroup; (c) and (d). Photomicrographs of the mafic dykes (*Abbreviations*: Opx, orthopyroxene; Chl, chlorite; Pl, plagioclase).

5. Results

5.1. Zircon LA-ICP-MS dating

Two groups of zircon grains from the Zhaiwa mafic dyke (ZW51) have been identified, i.e., coarse (100–150 μm) and euhedral grains (length-to-width ratios: 3:1–2:1) with obvious oscillatory magmatic zoning; fine (50–100 μm) and stubby grains with poor zoning (Fig. 4). It is noteworthy that most of the zircon grains analyzed are relatively smaller with the oscillatory magmatic zoning not so definite compared to those of typical felsic rocks. The chronological results are presented in Table 1 and Fig. 5.

The zircon grains have U and Th concentrations ranging 144–1025 ppm and 71–1255 ppm, respectively, with high Th/U values (0.26–1.55). The elevated Th/U values, together with the oscillatory magmatic zoning, indicate a magmatic origin for the analyzed zircon grains (Corfu et al., 2003; Wu and Zheng, 2004). The prismatic crystal shape, high U, Y, P and Ca contents and unimodal age indicate that the zircon grains from the Zhaiwa mafic dykes are not detritus grains while detrital zircon grains are generally rounded/subrounded with eroded margins, low U, Y, P and Ca contents and bi- or multimodal ages (Köppel and Sommerauer, 1974). It is noteworthy that the zircon grains from the Zhaiwa mafic dykes have wide zoning, indicating their formation in high temperature (because the temperatures affect diffusion rates of trace elements), which is consistent with typical zircon grains derived from mafic rocks (Corfu et al., 2003; Wu and Zheng, 2004). Twenty analyzed zircon grains from the Zhaiwa mafic dyke (ZW51) yielded a concordia age of 2235 ± 43 Ma (MSWD = 2.4) and a weighted mean $^{207}Pb/^{206}Pb$ age of 2242 ± 25 Ma (MSWD = 2.4). The two ages are within analytical uncertainty and we take the weighted mean $^{207}Pb/^{206}Pb$ age (2242 Ma) as the emplacement age of the Zhaiwa mafic dykes.

5.2. Zircon Lu–Hf isotopes

Analytical spots for the Hf isotope analyses are the same as those for the U–Pb dating and the results are summarized in Table 2 and Fig. 6.

The initial $^{176}Hf/^{177}Hf$ values of the zircon grains are calculated based on the U–Pb ages of the same zircon grain. The grains with Paleoproterozoic ages have initial $^{176}Hf/^{177}Hf$ values of 0.281012–0.281194 with negative $\varepsilon Hf(t)$ values ranging from −11.4 to −2.7 and T_{DM} ages ranging 2805–3051 Ma.

5.3. Whole-rock major and trace elements

The whole-rock major and trace element data are given in Table 3. The Zhaiwa mafic dykes may have undergone various degrees of sub-solidus alteration or low-grade metamorphism (hereinafter abbreviated as SALM) based on our petrographic observations and the LOI (Table 3). It is thus essential to evaluate the effects of SALM on the geochemistry of the Zhaiwa mafic dykes.

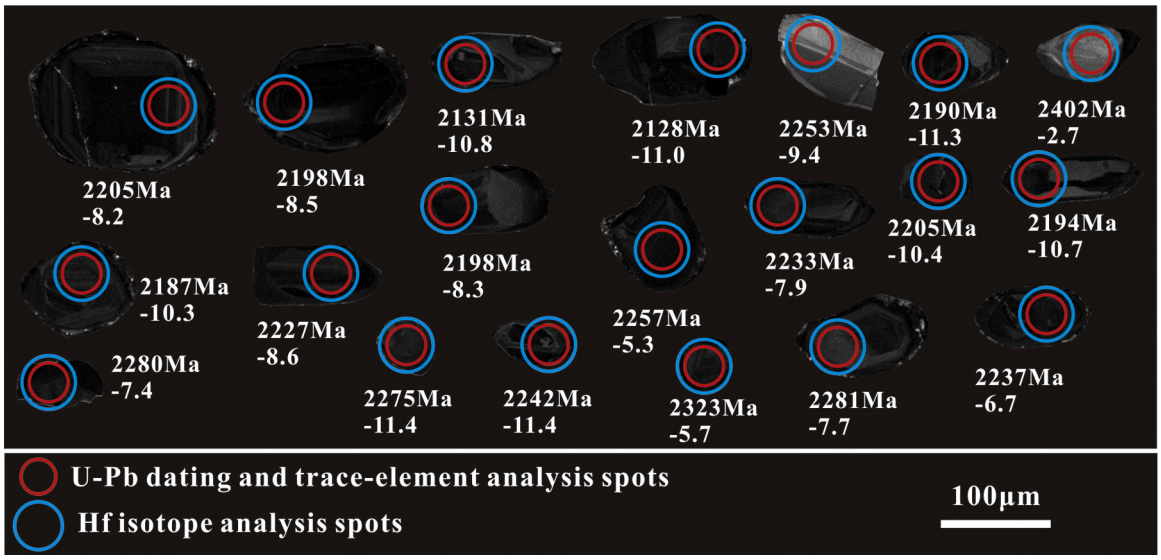

Fig. 4. Cathodoluminescence (CL) images of the analyzed zircons (sample ZW-51). Red circles denote U–Pb dating spots (32 μm) and blue circles denote Hf isotope analytical spots (44 μm).

Table 1
Zircon U–Pb dating results of the Zhaiwa mafic dykes.

Spot	PbTotal	Th (ppm)	U (ppm)	Th/U	$^{207}Pb/^{206}Pb$	±σ	$^{207}Pb/^{235}U$	±σ	$^{206}Pb/^{238}U$	±σ	$^{207}Pb/^{206}Pb$Age (Ma)	±σ
ZW51-01	248	397	377	1.05	0.1381	0.01	8.3139	0.53	0.4347	0.00	2205.6	108.3
ZW51-02	302	273	453	0.60	0.1377	0.01	9.0908	0.51	0.4772	0.01	2198.5	99.1
ZW51-03	391	659	617	1.07	0.1324	0.01	7.7393	0.38	0.4208	0.00	2131.5	81.8
ZW51-04	599	1237	891	1.39	0.1375	0.01	8.0907	0.33	0.4246	0.00	2198.2	69.8
ZW51-05	416	497	766	0.65	0.1323	0.00	7.5427	0.28	0.4103	0.01	2128.7	55.4
ZW51-06	358	266	616	0.43	0.1423	0.00	8.8564	0.21	0.4483	0.00	2257.4	42.1
ZW51-07	379	681	620	1.10	0.1367	0.00	7.6080	0.16	0.4012	0.00	2187.0	41.7
ZW51-08	437	539	694	0.78	0.1400	0.00	8.8072	0.18	0.4533	0.00	2227.5	33.5
ZW51-09	129	145	216	0.67	0.1421	0.00	8.8467	0.20	0.4496	0.01	2253.7	34.9
ZW51-10	598	1103	952	1.16	0.1370	0.00	7.8979	0.14	0.4151	0.00	2190.7	28.6
ZW51-11	373	416	661	0.63	0.1404	0.00	7.9347	0.11	0.4079	0.00	2233.0	24.1
ZW51-12	87	71	144	0.50	0.1550	0.00	9.5847	0.26	0.4457	0.01	2402.2	40.3
ZW51-13	384	289	711	0.41	0.1382	0.00	8.0732	0.13	0.4212	0.00	2205.6	24.4
ZW51-14	519	1255	808	1.55	0.1373	0.00	7.5177	0.12	0.3951	0.00	2194.4	25.8
ZW51-15	337	233	598	0.39	0.1444	0.00	8.5151	0.14	0.4256	0.00	2280.6	27.8
ZW51-16	384	651	549	1.19	0.1444	0.00	8.9308	0.15	0.4466	0.00	2281.2	27.6
ZW51-17	337	403	581	0.69	0.1481	0.00	8.4589	0.17	0.4118	0.00	2323.8	29.2
ZW51-18	404	495	778	0.64	0.1408	0.00	7.1587	0.13	0.3673	0.00	2236.7	29.9
ZW51-19	305	164	626	0.26	0.1439	0.00	7.6331	0.25	0.3870	0.01	2275.9	43.1
ZW51-20	434	653	835	0.78	0.1413	0.00	7.4465	0.18	0.3811	0.01	2242.9	33.0

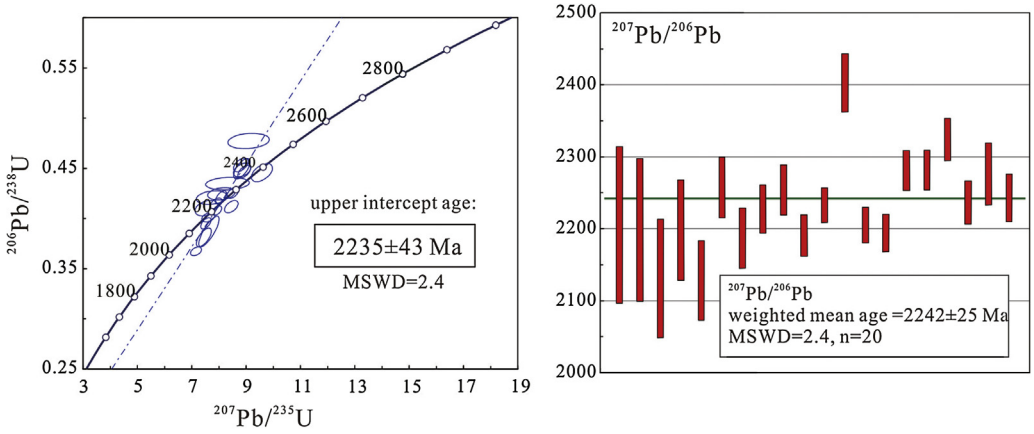

Fig. 5. Zircon U–Pb concordia diagram for the Zhaiwa mafic dykes (ZW51).

Table 2
Hf isotope of zircon grains from the Zhaiwa mafic dykes.

Spot	$^{176}Yb/^{177}Hf$	1σ	$^{176}Lu/^{177}Hf$	1σ	$^{176}Hf/^{177}Hf$	1σ	$(^{176}Hf/^{177}Hf)_i$	t (Ma)	εHf(0)	εHf(t)	T_{DM1} (Ma)	$f_{Lu/Hf}$	T_{DM2} (Ma)
ZW51-01	0.032235	0.000407	0.000837	0.000007	0.281181	0.000008	0.281146	2205	−56.3	−8.2	2872	−0.97	3137
ZW51-02	0.033384	0.000212	0.000908	0.000007	0.281181	0.000008	0.281143	2198	−56.3	−8.5	2877	−0.97	3145
ZW51-03	0.037077	0.000204	0.001157	0.000009	0.281168	0.000009	0.281121	2131	−56.7	−10.8	2913	−0.97	3214
ZW51-04	0.041377	0.000166	0.001121	0.000006	0.281194	0.000008	0.281147	2198	−55.8	−8.3	2876	−0.97	3137
ZW51-05	0.025903	0.000177	0.000785	0.000006	0.281149	0.000008	0.281117	2128	−57.4	−11.0	2911	−0.98	3223
ZW51-06	0.028848	0.000161	0.000763	0.000006	0.281227	0.000008	0.281194	2257	−54.7	−5.3	2805	−0.98	3023
ZW51-07	0.038009	0.000475	0.001065	0.000009	0.281142	0.000008	0.281098	2187	−57.6	−10.3	2941	−0.97	3234
ZW51-08	0.044495	0.000411	0.001262	0.000017	0.281175	0.000010	0.281121	2227	−56.5	−8.6	2912	−0.96	3173
ZW51-09	0.024443	0.000346	0.000801	0.000016	0.281115	0.000011	0.281081	2253	−58.6	−9.4	2958	−0.98	3238
ZW51-10	0.050119	0.000287	0.001564	0.000014	0.281135	0.000010	0.281069	2190	−57.9	−11.3	2991	−0.95	3287
ZW51-11	0.034291	0.000177	0.001100	0.000008	0.281183	0.000008	0.281136	2233	−56.2	−7.9	2889	−0.97	3143
ZW51-12	0.012840	0.000088	0.000402	0.000004	0.281191	0.000008	0.281173	2402	−55.9	−2.7	2826	−0.99	3001
ZW51-13	0.049355	0.000583	0.001492	0.000022	0.281147	0.000009	0.281085	2205	−57.4	−10.4	2967	−0.96	3251
ZW51-14	0.030789	0.000342	0.000927	0.000011	0.281121	0.000010	0.281082	2194	−58.4	−10.7	2959	−0.97	3260
ZW51-15	0.031574	0.000132	0.001018	0.000006	0.281166	0.000009	0.281121	2280	−56.8	−7.4	2906	−0.97	3150
ZW51-16	0.033699	0.000087	0.000905	0.000005	0.281151	0.000007	0.281112	2281	−57.3	−7.7	2917	−0.97	3168
ZW51-17	0.034227	0.000285	0.001082	0.000011	0.281188	0.000009	0.281140	2323	−56.0	−5.7	2881	−0.97	3097
ZW51-18	0.037221	0.000663	0.001232	0.000024	0.281219	0.000009	0.281166	2237	−54.9	−6.7	2850	−0.96	3084
ZW51-19	0.024941	0.000144	0.000824	0.000005	0.281048	0.000023	0.281012	2275	−61.0	−11.4	3051	−0.98	3359
ZW51-20	0.046983	0.000846	0.001551	0.000024	0.281099	0.000015	0.281033	2242	−59.1	−11.4	3038	−0.95	3333

Note: $\varepsilon_{Hf}(0) = 10{,}000*[(^{176}Hf/^{177}Hf)_S/(^{176}Hf/^{177}Hf)_{CHUR,0} - 1]$, $f_{Lu/Hf} = (^{176}Lu/^{177}Hf)_S/(^{176}Lu/^{177}Hf)_{CHUR} - 1$.
$\varepsilon_{Hf}(t) = 10{,}000*\{[(^{176}Hf/^{177}Hf)_S - (^{176}Lu/^{177}Hf)_S*(e^{\lambda t} - 1)]/[(^{176}Hf/^{177}Hf)_{CHUR,0} - (^{176}Lu/^{177}Hf)_{CHUR}*(e^{\lambda t} - 1)] - 1\}$.
T_{DM1} is one-stage Hf model age, calculated as $T_{DM1} = 1/\lambda*\ln\{(1 + [(^{176}Hf/^{177}Hf)_S - (^{176}Hf/^{177}Hf)_{DM}]/[(^{176}Lu/^{177}Hf)_S - (^{176}Lu/^{177}Hf)_{DM}]\}$. T_{DM2} is two-stage Hf model age, calculated as $T_{DM2} = T_{DM1} - (T_{DM1} - t)*(f_{cc} - f_s)/(f_{cc} - f_{DM})]$.
Where, $\lambda = 1.867 \times 10^{-11}$ year^{-1} (Söderlund et al., 2004); $(^{176}Lu/^{177}Hf)_S$ and $(^{176}Hf/^{177}Hf)_S$ are the measured values of samples; $(^{176}Lu/^{177}Hf)_{CHUR} = 0.0332$ and $(^{176}Hf/^{177}Hf)_{CHUR,0} = 0.282772$ (Blichert-Toft and Albarède, 1997); $(^{176}Lu/^{177}Hf)_{DM} = 0.0384$ and $(^{176}Hf/^{177}Hf)_{DM} = 0.28325$ (Griffin et al., 2000); $(^{176}Lu/^{177}Hf)$mean crust = 0.0115 (Wang et al., 2009); $f_{cc} = [(^{176}Lu/^{177}Hf)$mean crust$/(^{176}Lu/^{177}Hf)_{CHUR}] - 1$; $f_s = f_{Lu/Hf}$, $f_{DM} = [(^{176}Lu/^{177}Hf)_{DM}/(^{176}Lu/^{177}Hf)_{CHUR}] - 1$; t = crystallization time of zircon.

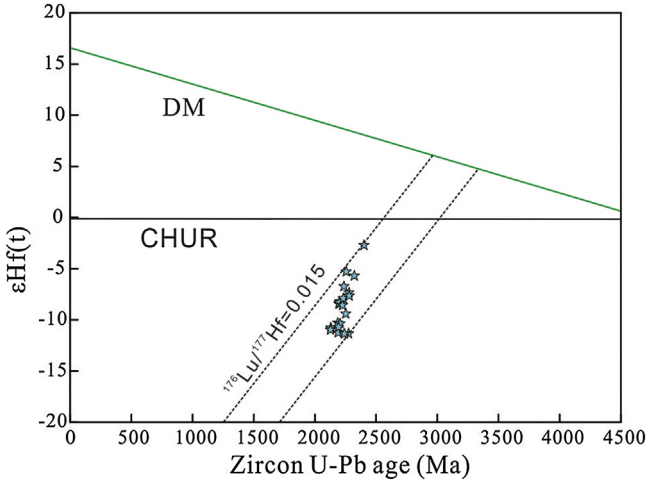

Fig. 6. Zircon Hf isotopic compositions of the Zhaiwa mafic dykes (ZW51).

Zirconium is one of the most immobile elements inert to SALM processes (Wood and Blundy, 1997; Hodson, 2002). Thus, correlations between Zr and other elements can be used to evaluate these elements' mobility under SALM (Hodson, 2002; Polat et al., 2002). The linear correlations between Zr and some alkaline-earth elements (e.g., Ba; Fig. 7), HFSEs (e.g., Nb, Hf; Fig. 7), REEs (e.g., La, Sm, Eu and Y; Fig. 7), suggest that these elements in the Zhaiwa mafic dykes were relatively immobile to SALM (Polat et al., 2002). Therefore, SALM influence on the geochemistry of the Zhaiwa mafic dykes was minimal except for some LILEs (e.g., K and Rb; Fig. 7). The Zhaiwa mafic dykes have 47.92–56.17 wt% SiO_2. Some samples (11ZW02) have higher SiO_2 content (56 wt%) than mafic rocks, possibly due to hydrothermal alteration. Concentrations of MgO range 2.93–7.02 wt%, with $Mg^{\#}$ ($Mg^{\#} = Mg^{2+}/(Mg^{2+} + Fe^{2+})$) values of 46–61. Most samples plot in the fields of basalt and basaltic andesite in the TAS diagram (Fig. 8a; Le Bas et al., 1986). It is a reasonable assumption that some mobile elements (e.g., Na and K) may have been remobilized by later alteration based on the moderate to high loss on ignition (LOI). Here, we adopt the Zr–TiO_2 vs. Nb/Y diagram to characterize the Zhaiwa mafic dykes, which plot in the fields of andesite and basalt (Fig. 8b; Winchester and Floyd, 1977). In the ($FeO + Fe_2O_3 + TiO_2$)–Al_2O_3–MgO ternary diagram (Jensen, 1976), the Zhaiwa mafic dykes plot in the field of high-Fe tholeiitic basalt (Fig. 8c). MgO shows clear positive correlation with CaO and negative correlations with TiO_2 and P_2O_5 (Fig. 9).

As seen in the chondrite-normalized rare earth element (REE) patterns, the Zhaiwa mafic dykes contain less enriched light REEs (LREEs) than the average ocean island basalts (OIB) but more enriched LREEs than the average enriched mid-ocean-ridge basalt (E-MORB). Meanwhile, the Zhaiwa mafic dykes contain more enriched heavy REEs (HREEs) than the OIB but mimic average E-MORB (Fig. 10a). The weak negative Eu anomalies may suggest minor plagioclase fractional crystallization. In the primitive-mantle normalized spider diagram, the samples show clear negative anomalies of high field strength elements (HFSEs, e.g., Nb, Ta, Ti, P) and wide range of large ion lithophile elements (LILEs), resembling typical Andean-type magmatism (Fig. 10b; Xu et al., 2008).

5.4. Whole-rock Sr–Nd isotopes

Whole rock Sr–Nd isotopic composition data for the Zhaiwa mafic dykes are listed in Table 4. The $(^{87}Sr/^{86}Sr)_t$ (t = 2242 Ma) data have been divided into two groups, i.e., 0.705605–0.707058 and 0.725237–0.748725. This phenomenon is probably caused by hydrothermal alteration, as hydrothermal alteration can lead to the migration of Rb (Fig. 7) and inaccuracy of Sr isotopes. The samples have $\varepsilon Nd(t)$ values ranging from −6.67 to −3.27, with the corresponding T_{DM} ages of 3020–4063 Ma.

6. Discussion

According to the large age discrepancy between the Zhaiwa Mo mineralization (~1.76 Ga; Deng et al., 2013a,b) and the Zhaiwa mafic intrusion (~2.24 Ga), direct metallogenic association appears unlikely between them. Nevertheless, our work can shed light on

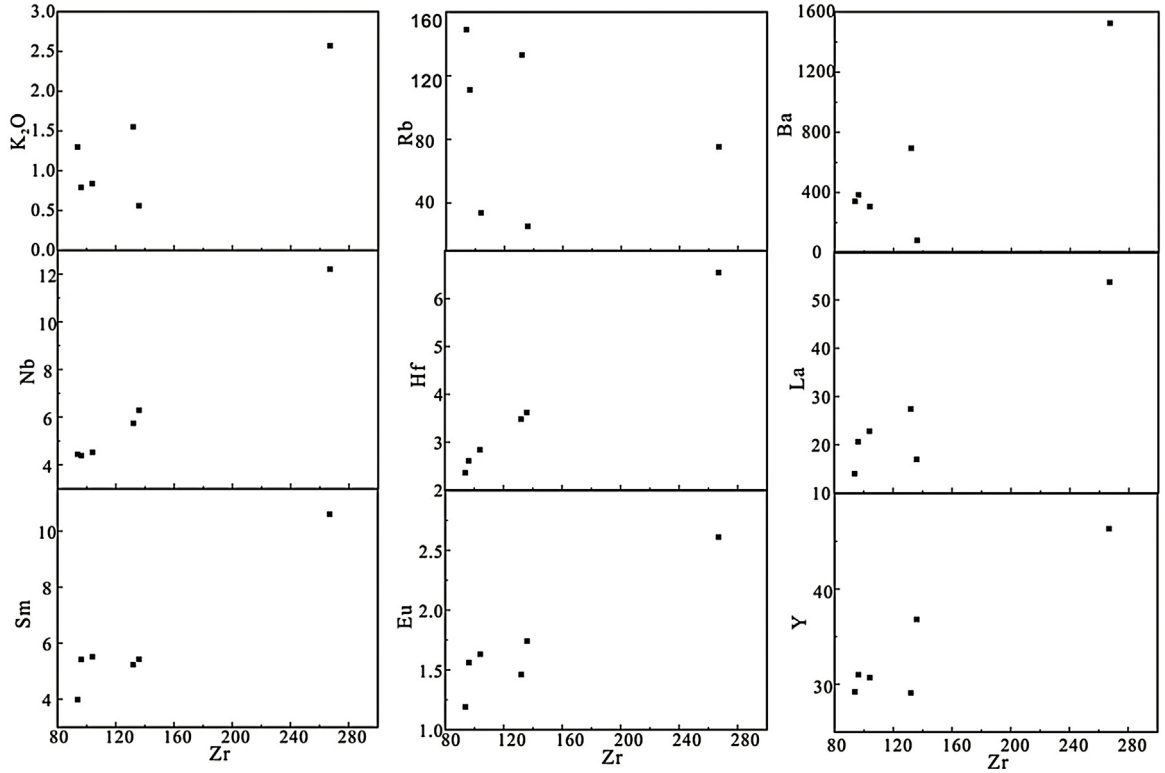

Fig. 7. Major and trace element plots against Zr (as fractionation index) for the Zhaiwa mafic dykes.

regional tectonic evolution. This is because mantle-derived mafic rocks record the age and geochemistry, and thus the geodynamic history, of the mantle.

6.1. Petrogenesis of the Zhaiwa mafic dykes

Crustal contamination, fractional crystallization and partial melting may have been responsible for the formation of the Zhaiwa mafic dykes. The relative importance of these processes is discussed below.

6.1.1. Crustal contamination

Mantle derived melts are inevitably affected by crustal contamination during their ascent through continental crust (Castillo et al., 1999). The Zhaiwa mafic dykes may have been subjected to certain degrees of crustal continuation due to their depletion in Nd and Ta, which are generally depleted in crustal rocks compared to other strongly incompatible elements (Kampunzu et al., 2003; Lana et al., 2004). Crustal contamination gives rise to an increase in $(^{87}Sr/^{86}Sr)_i$ and a decrease of $\varepsilon Nd(t)$ (Rogers et al., 2000), due to the relatively low $\varepsilon Nd(t)$, MgO, $(Nb/La)_{PM}$, Nb/Th, Sm/Nd and high $^{87}Sr/^{86}Sr$ (Rudnick, 1995). Thus, rocks subjected to intense crustal contamination commonly possess low contents of $\varepsilon Nd(t)$, MgO, and Sm/Nd. It seems that no significant crustal contamination occurred during magma ascent, given the absence of correlations between $Mg^{\#}$ and $\varepsilon Nd(t)$ (Fig. 11a), or between $\varepsilon Nd(t)$ and Sm/Nd (Fig. 11b). This inference is further supported by: (1) As a strongly incompatible element, thorium is enriched in sediments and mid-upper crust (average Th concentrations in the middle- and upper crust are ~6.5 and 10.5 ppm, respectively; Rudnick and Gao, 2003). However, thorium is relatively low in the Zhaiwa mafic dykes (0.77–2.41 ppm), precluding the involvements of middle- or upper crustal materials in the genesis of the Zhaiwa mafic dykes; (2) The Zhaiwa mafic dykes show generally limited range of $(Nb/La)_{PM}$ (0.19–0.35). But this ratio is 0.6 for the lower crust and 0.37 for the upper crust, respectively (Rudnick and Gao, 2003). (3) Because the Zhaiwa mafic dykes show enriched istopes, so when considering the Pb compositions, considerable amount of crustal materials would be required if we assume that the Zhaiwa mafic dykes were derived from an E-MORB-like source (0.6 ppm; Rudnick and Gao, 2003) with the interaction of upper crustal materials (17 ppm; Rudnick and Gao, 2003). If this substantial crustal contamination had occurred, the resulting rocks would be intermediate to felsic, instead of mafic.

To summarize, crustal contamination may not have played a significant role in the petrogenesis of the Zhaiwa mafic dykes.

6.1.2. Fractional crystallization

From the variable major and trace element compositions, the parental magma of the Zhaiwa mafic dykes should have undergone certain degrees of fractional crystallization. The largely linear correlation between Al_2O_3 and CaO (Fig. 9c), combined with the minor negative Eu anomaly (Fig. 10a), indicate that fractional crystallization of plagioclase had occurred. Clinopyroxene fractionation is evidenced from the positive correlation between CaO and MgO. In contrast, extensive fractional crystallization of Fe–Ti oxides may have been absent as there lacks common correlations among TiO_2, Fe_2O_3 and MgO (Fig. 9d and f).

6.1.3. Partial melting

Partial melting was likely to have predominated, over crustal contamination and fractional crystallization, to control the geochemistry of the Zhaiwa mafic dykes (Fig. 12; Allegre and Minster, 1978).

The Zhaiwa mafic dykes are characterized by negative Nb and Ta anomalies, which can be led by: (1) crustal contamination (Rudnick and Gao, 2003); (2) contribution of recycled crustal sediments (Hawkesworth et al., 1993); (3) subduction-related fluid metasomatism (Donnelly et al., 2004); (4) fractional crystallization of Ti-rich minerals (such as rutile or ilmenite) (Huang et al., 2010).

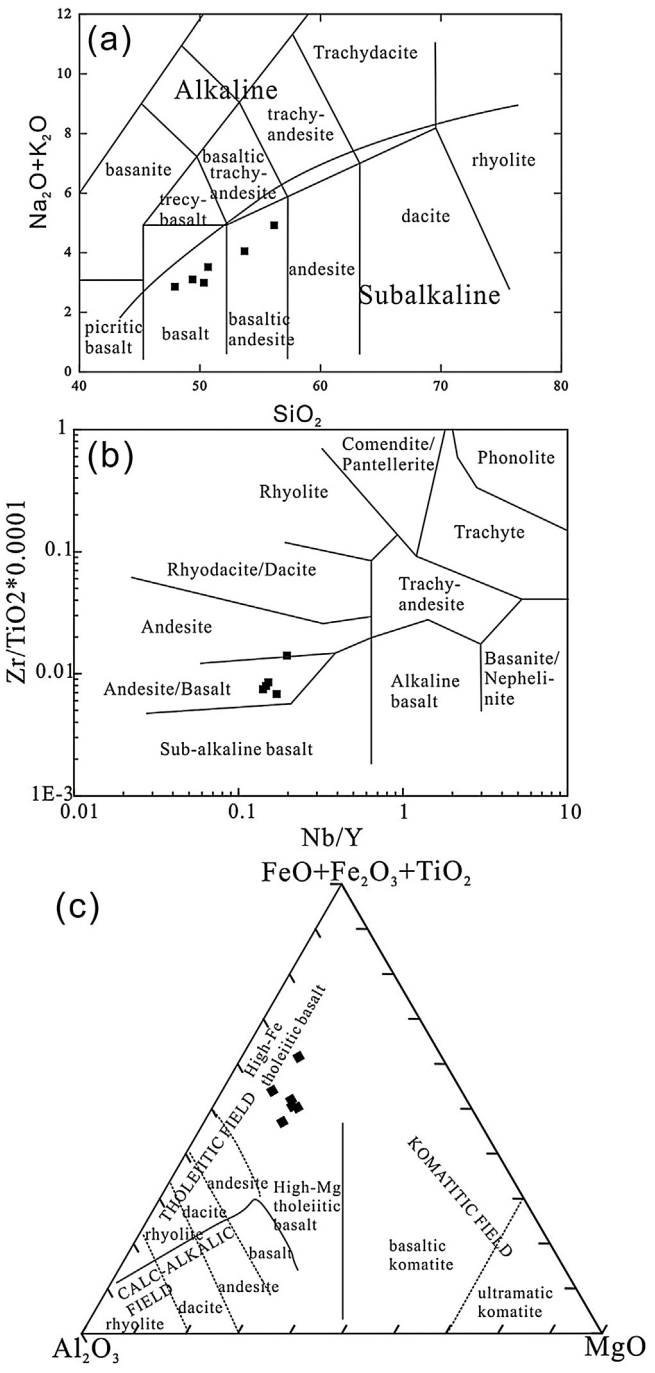

Fig. 8. (a) ($K_2O + Na_2O$) vs. SiO_2 diagram (after Middlemost, 1994); (b) Zr/TiO_2 vs. Nb/Y diagram (Winchester and Floyd, 1977); (c) ($FeO + Fe_2O_3 + TiO_2$)–Al_2O_3–MgO diagram (Jensen, 1976).

Table 3
Whole rock geochemistry for the Zhaiwa mafic dykes.

Sample	11ZW02	11ZW03	11ZW08	11ZW09	11ZW10	11SG01
SiO_2	56.17	50.33	49.4	53.7	50.68	47.92
TiO_2	1.68	1.29	1.11	0.94	1.31	2.00
Al_2O_3	13.99	14.65	14.36	15.12	14.92	12.24
Fe_2O_3	11.29	12.56	12.37	10.79	12.31	16.63
FeO	7.85	8.75	8.2	7.1	8.5	8.85
MnO	0.16	0.22	0.19	0.16	0.19	0.19
MgO	3.71	6.21	7.02	6	6.64	4.87
CaO	6.32	8.71	10.48	6.66	7.32	8.01
Na_2O	2.35	2.2	1.8	2.49	2.68	2.3
K_2O	2.57	0.79	1.3	1.55	0.84	0.56
P_2O_5	0.54	0.39	0.16	0.23	0.40	0.32
LOI	1.2	2.53	1.78	2.31	2.66	4.87
Total	99.97	99.88	99.97	99.94	99.95	99.91
$Mg^{\#}$	45.97	56.09	60.65	60.34	58.44	49.76
Sc	23.7	32.2	41.5	27.2	32.1	38.9
V	164	189	261	145	191	367
Cr	128	291	206	257	294	34.8
Co	28.2	39.3	41.6	34.7	42.5	43.6
Ni	38.2	90.7	76.5	72.0	126	42.7
Ga	21.3	18.3	17.6	17.4	17.9	18.2
Rb	75.3	111	149	133	33.8	25.3
Sr	429	373	192	288	288	365
Y	46.3	31.0	29.2	29.1	30.7	36.8
Zr	267	96.3	93.9	132	104	136
Nb	12.2	4.38	4.44	5.74	4.52	6.29
Cs	3.17	4.57	1.53	4.20	0.86	5.43
Ba	1524	385	342	694	307	81.9
La	53.7	20.6	14.0	27.4	22.8	16.9
Ce	113	45.1	23.9	54.9	49.3	37.9
Pr	13.9	5.78	3.68	6.93	6.42	4.98
Nd	55.2	25.1	15.3	27.5	27.0	21.9
Sm	10.6	5.41	3.98	5.23	5.51	5.42
Eu	2.61	1.56	1.19	1.46	1.63	1.74
Gd	8.95	5.15	4.38	5.00	5.47	6.09
Tb	1.38	0.83	0.80	0.79	0.85	1.03
Dy	7.82	5.08	4.95	4.84	5.29	6.45
Ho	1.55	1.03	1.05	1.00	1.03	1.33
Er	4.29	2.96	2.88	2.84	2.98	3.77
Tm	0.62	0.42	0.42	0.42	0.43	0.56
Yb	4.11	2.92	2.75	2.72	2.85	3.55
Lu	0.61	0.44	0.41	0.42	0.44	0.55
Hf	6.54	2.61	2.36	3.48	2.84	3.62
Ta	0.63	0.28	0.27	0.32	0.28	0.35
Pb	12.9	8.17	5.65	4.22	3.04	6.06
Th	2.41	0.77	1.32	2.03	0.99	1.62
U	0.45	0.19	0.59	0.34	0.24	0.36

As discussed above, crustal contamination and fractional crystallization may not have played an important role in the genesis of the Zhaiwa mafic dykes. A mantle source metasomatized by slab fluids/melts is also unlikely (Plank, 2005). This is because mafic rocks formed from a metasomatized mantle source (e.g., mantle wedge) are characterized by high Sr, La/Yb and low HREE (e.g., Y), as well as $\varepsilon Nd(t)$ and $\varepsilon Hf(t)$ similar to those of MORB, consistent with the quasi-adakite (Martin et al., 2005; Guo et al., 2007). Although the Zhaiwa mafic dykes have high Sr and low Y, they have extremely low La/Yb and very different $\varepsilon Nd(t)$ and $\varepsilon Hf(t)$ with those of MORB. Hence, contributions from slab fluids/melts can also be precluded.

The Th/Yb vs. Ba/La diagram (Woodhead et al., 2001) can be used to distinguish slab-derived fluid input from sediment one. We

Table 4
Whole rock Sr and Nd isotope data for the Zhaiwa mafic dykes.

Samples	Rb (ppm)	Sr (ppm)	$^{87}Rb/^{86}Sr$	$^{87}Sr/^{86}Sr$	$\pm 2\sigma$	I_{Sr}	Sm (ppm)	Nd (ppm)	$^{147}Sm/^{144}Nd$	$^{143}Nd/^{144}Nd$	$\pm 2\sigma$	$\varepsilon Nd(t)$	T_{DM} (Ma)
11ZW03	111	373	0.839	0.775873	7	0.748725	5.41	25.10	0.136	0.511492	3	−4.85	3228
11ZW08	149	192	2.189	0.796033	5	0.725237	3.98	15.30	0.164	0.511814	6	−6.67	4063
11ZW10	33.8	288	0.331	0.716312	4	0.705605	5.51	27.00	0.129	0.511456	6	−3.46	3020
11SG01	25.3	365	0.195	0.713381	4	0.707058	5.42	21.90	0.156	0.511870	6	−3.27	3362

Note: $\varepsilon Nd(t) = [(^{143}Nd/^{144}Nd)_S/(^{143}Nd/^{144}Nd)_{CHUR} - 1] \times 10{,}000$. $T_{DM} = \ln[(^{143}Nd/^{144}Nd)_S - (^{143}Nd/^{144}Nd)_{DM}]/[(^{143}Sm/^{144}Nd)_S - (^{147}Sm/^{144}Nd)_{DM}]/\lambda$ (DePaolo, 1988). In the calculation, $(^{143}Nd/^{144}Nd)_{CHUR} = 0.512638$, $(^{147}Sm/^{144}Nd)_{CHUR} = 0.1967$, $(^{143}Nd/^{144}Nd)_{DM} = 0.51315$, $(^{147}Sm/^{144}Nd)_{DM} = 0.2136$, $t = 2242$ Ma.

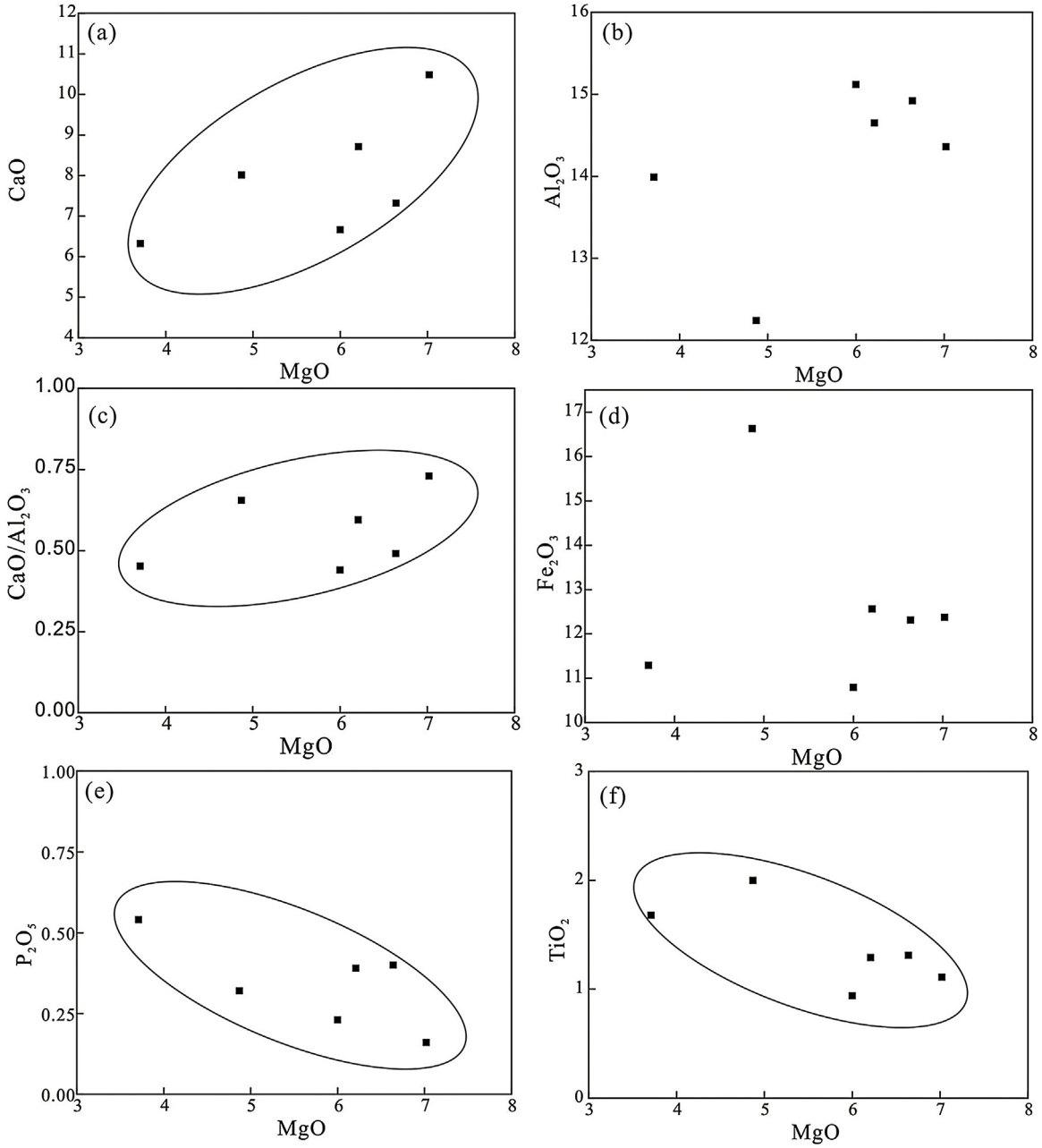

Fig. 9. Major and trace element plots against MgO (as fractionation index) for the Zhaiwa mafic dykes.

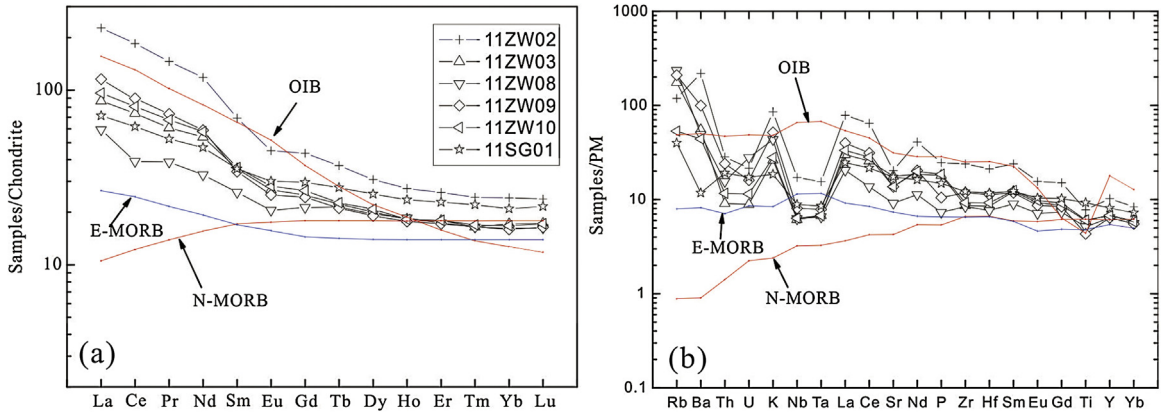

Fig. 10. (a) Chondrite-normalized REE diagram and; (b) primitive mantle-normalized multi-element diagram for the Zhaiwa mafic dykes. Average compositions of chondrite, primitive mantle, OIB (ocean island basalts), E-MORB (enriched MORB) and N-MORB (normal MORB) are from Sun and McDonough (1989).

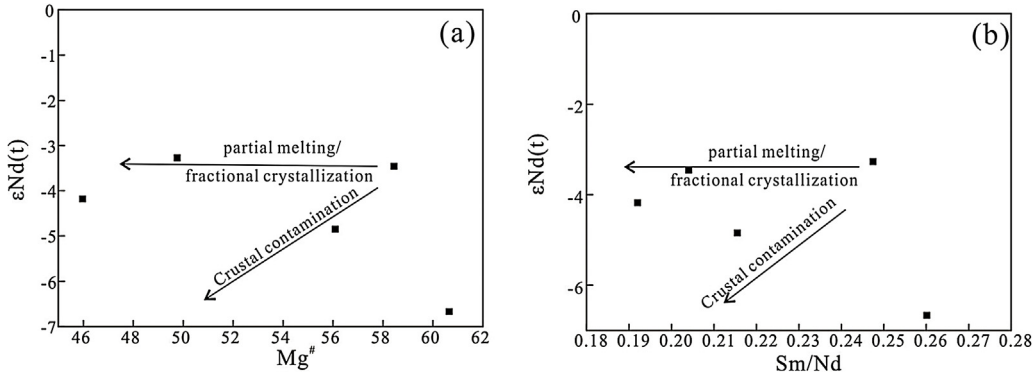

Fig. 11. (a) $\varepsilon Nd(t)$ vs. $Mg^{\#}$ diagram; (b) $\varepsilon Nd(t)$ vs. Sm/Nd diagram.

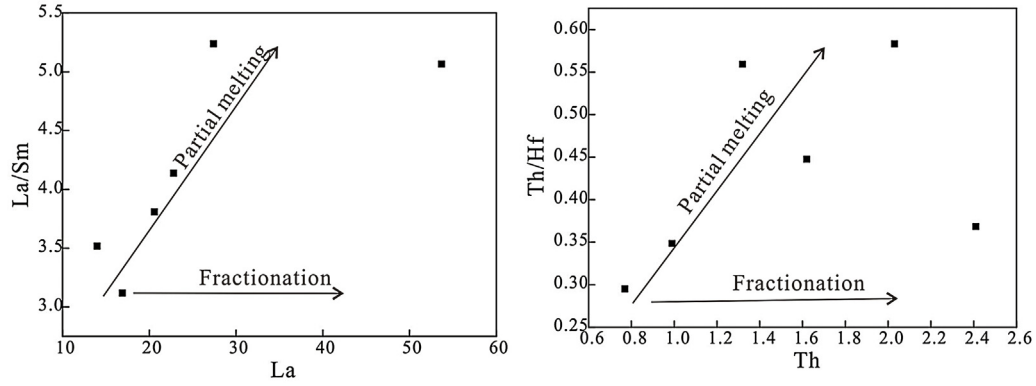

Fig. 12. (a) La/Sm vs. La diagram; (b) Th/Hf vs. Th diagram (after Allegre and Minster, 1978).

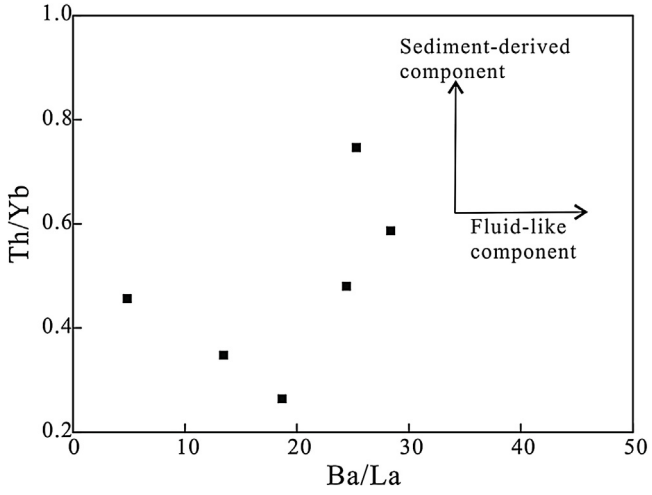

Fig. 13. Th/Yb vs. Ba/La diagram (after Woodhead et al., 2001).

suggest that sediments, not slab-derived fluids, contributed to the parental magmas of the Zhaiwa mafic dykes (Fig. 13).

Geochemical signatures of the Zhaiwa mafic dykes, e.g., low TiO_2 (0.94–2.00 wt%) and enriched Sr–Nd isotopes argue against an asthenospheric mantle source, which generally produce magmatic rocks with high TiO_2 (average TiO_2 in OIB: 2.86 wt%) and depleted Sr–Nd isotopes (Lightfoot et al., 1993; Wu et al., 2014; Fig. 14a). Thus, a sub-continental lithospheric mantle (SCLM) source modified by contribution of recycled terrigenous sediments is likely. The slight LREE/HREE enrichment of the Zhaiwa mafic dykes may have been derived either by a high degree of partial melting of garnet-bearing mantle source or by partial melting of spinel-bearing mantle source at a shallow depth (<70 km; Menzies and Chazot, 1995). In the Sm/Yb vs. La/Sm diagram (Fig. 14b), the Zhaiwa mafic dykes lie along the mixing curve between melt derived from ~5% melting of a source with ~1% residual garnet and ~1% melting of a source with ~3% residual garnet. In summary, simulation calculation reveals that nearly no garnet exist in the mantle source, implying a relatively shallow depth.

6.2. Tectonic setting and geodynamic implications on the Trans-North China Orogen

As shown above, the Zhaiwa mafic dykes plot in the field of high-Fe tholeiitic basalt (Fig. 8c). The high Fe contents can be obtained from: (1) up-welling mantle plume (Gibson et al., 2000); (2) garnet-bearing lherzolite (Takahahshi et al., 1998); (3) mantle-wedge metasomatized by slab-derived fluids/melts (Leybourne et al., 1999); (4) garnet-free refractory mantle (Hanski and Smolkin, 1995). Although mafic dyke swarms dated at ~2.2 Ga were found globally in recent years and perhaps were related with mantle plumes (French and Heaman, 2010), the genesis of the Zhaiwa mafic dykes was unlikely to be associated with mantle plumes, because: (1) the Zhaiwa mafic dykes are only sparsely distributed, inconsistent with the widespread mafic rocks associated with mantle plumes; (2) plume-related basalts are generally enriched in Nb, Ta and have high Ce/Pb ratios (Callegaro et al., 2013), which is inconsistent with the Zhaiwa mafic dykes; (3) the calculated mantle potential temperatures (Tp) via the formula Tp = 1463 + 12.74MgO–2924/MgO (MgO in wt%) range 722–1135 °C (Herzberg et al., 2007; Herzberg and Asimow, 2008; Herzberg and Gazel, 2009), which is clearly lower that that related to mantle plume (i.e., 1560–1620 °C for the Galapagos mantle plume; Herzberg and Asimow, 2008).

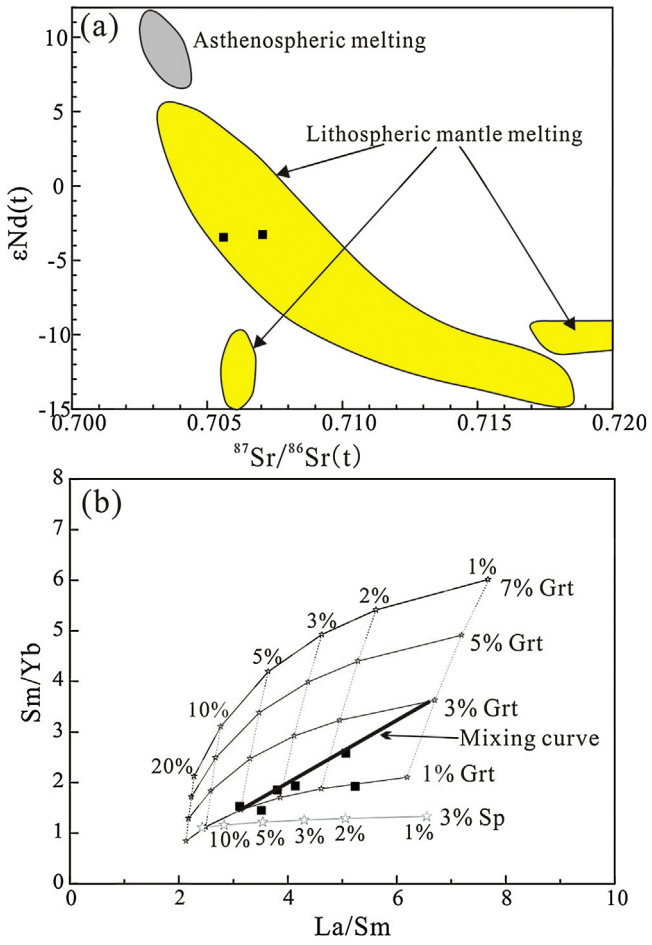

Fig. 14. (a) $\varepsilon Nd(t)$ vs. $^{87}Sr/^{86}Sr(t)$ diagram (modified after Wu et al., 2014); (b) Sm/Yb vs. La/Sm diagram and non-modal batch melting (Shaw, 1970) of a lherzolitic mantle source. Partition coefficients are from McKenzie and O'Nions (1991). The black curves represent the melting curves of garnet-bearing lherzolite mantle source containing a spectrum of garnet contents (Kinzler, 1997). The gray curve represents the melting curve of a spinel-bearing lherzolite source containing a spectrum of spinel contents (Hellebrand et al., 2002). The bold line represents the mixing curve. *Abbreviations*: Grt, garnet; Sp, spinel.

Mafic rocks derived from a metasomatized mantle source (e.g., mantle wedge) have geochemical characteristics of quasi-adakite (Guo et al., 2007; Martin et al., 2005), contrary to the case of the Zhaiwa mafic dykes. On the other hand, simulation calculation reveals that nearly no garnet exists in the mantle source, arguing against the garnet-bearing lherzolite as a possible source. Based on the above evidence, the only feasible source for the Zhaiwa mafic dykes is garnet-free refractory mantle. The enriched isotopes may be the result of metasomatism related to previous subduction-collision.

Zhao et al. (2009) proposed that the Trans-North China Orogen (TNCO) may represent a long-lived continental margin arc (>650 Ma), although it remains unclear whether the southern North China Craton margin also underwent such a long-lived subduction. In fact, the southern segment of the TNCO had experienced at least three episodes of crustal accretion (during 2.85–2.72, 2.57–2.48 and 2.34–2.30 Ga) before the emplacement of the Zhaiwa mafic dykes (Huang et al., 2013), which may have led to the enrichment of the SCLM. To integrate with the minor LREE/HREE enrichment and simulation calculations of the Zhaiwa mafic dykes, which imply the absence of garnet in the mantle source (Fig. 14b), we conclude that the Zhaiwa mafic dykes were formed at a relatively shallow depth (<70 km), and were in an extensional setting, e.g., back-arc rifting.

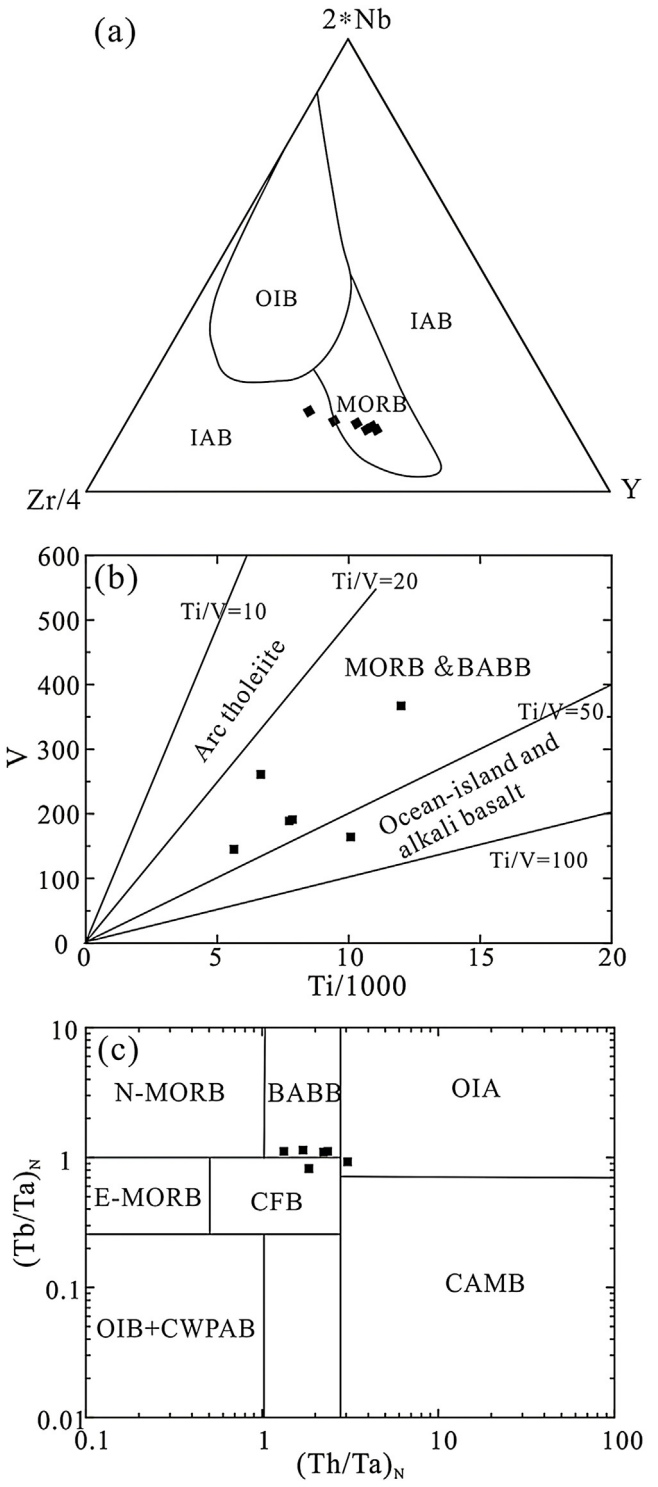

Fig. 15. (a) Quadratic discriminant analysis of the Zr–Y–Nb system (Vermeesch, 2006); (b) TiO_2 vs. V diagram (Wang et al., 2013); (c) $(Th/Ta)_N$ vs. $(Tb/Ta)_N$ (Zhang et al., 2013). OIB, ocean island basalts; IAB, island arc basalts; BABB, back-arc basin basalts; OIA, Mariana-type intra-oceanic arc; CAMB, active continental margin basalts; CFB, continental flood basalts; CWPAB, continental within-plate alkali and transitional basalts.

As stated above, the samples show clear negative anomalies of high field strength elements (HFSEs, e.g., Nb, Ta, Ti, P) and wide range of large ion lithophile elements (LILEs). Although both back-arc basin basalts and island arc basalts may have this features, the composition of back-arc basin basalts are intermediate between

MORB and IAB (island arc basalts) (Pearce and Stern, 2006). As seen in Fig. 15a, the Zhaiwa mafic dykes are plotted in the transition fields between MORB and IAB, indicating a back arc setting more probable. Moreover, island arc basaltic rocks are more oxidized than basalts of other settings and will generate higher V contents and lower Ti/V ratios (Kelley and Cottrell, 2012; Shervais, 1982). Therefore, the relative lower V contents and higher Ti/V ratios, distinct from arc basalts, show that the Zhaiwa mafic dykes are in a back arc setting (Fig. 15b), which can be further confirmed in Fig. 15c. Meanwhile, the Zhaiwa mafic dykes have $(La/Yb)_N$ values of 3.4–9.3, Ba/La ratios of 13–28 and Sm/Nd ratios of 0.19–0.26, consistent with intra-continental back arc basalts which typically exhibit $(La/Yb)_N > 3$, Ba/La > 10 and Sm/Nd < 0.3 (Fan et al., 2010). Although coeval arc-related rocks have not been identified, their existence cannot be precluded due to lacking detailed regionla geochemical survey. Then our studies in the Zhaiwa mafic dykes in the Taihua Complex is consistent with Liu et al. (2014a,b) in Lvliang Complex, which suggest an overall 2.2–2.1 Ga back-arc setting in the Lvliang Complex, adding more evidence implying that the southern North China Craton margin also underwent a long-lived subduction.

In Section 1, we have stated that three controversial models have been arised regarding the formation of the TNCO. The above discussion show that the Zhaiwa mafic dykes were emplaced in a intra-continental back arc setting at ~2.2 Ga, showing that final collision between the Western and Eastern Blocks no earlier than 2.2 Ga. Then the model advocating the final amalgamation resulted from a westward subduction at ~2.5 Ga (later modified to 2.3–2.2 Ga) can be precluded. In order to further discriminate the other two models, to clarify the geodynamic settings of the tectonic events at ~2.1 Ga is essential. In fact, ~2.1 Ga igneous rocks are ubiquitous in the TNCO, such as the mafic dykes in the Lvliang Complex (Wang et al., 2014), the Xuting potassic granite in the Zanhuang Complex (Yang et al., 2011), the Lingyunkou potassic granite in the Hengshan Complex (Zhao et al., 2011), the Huangjinshan potassic granite and A_1-type granite in the Wutai Complex (Du et al., 2012), and the quartz-monzonite porphyry in the Zhongtiao Complex (Li et al., 2013). Two tectonic settings have been arised to account for the ~2.1 Ga igneous rocks between a continental rift and a back arc basin. We are not sure which setting is more appropriate to interpret the petrogenesis of these ~2.1 Ga igneous rocks, but both these two models suggest extension rather than collision. Although we cannot determine the polarity of subduction, a westward subduction with two Paleoproterozoic collisions at ~2.1 Ga and ~1.85 Ga can be excluded. Then, an eastward subduction with the final amalgamation at ~1.85 Ga may be the best model to explain the formation of the TNCO.

7. Conclusion

1. The intrusion age of the Zhaiwa mafic dykes are ~2.24 Ga. According to the large age discrepancy between the Zhaiwa Mo mineralization (~1.76 Ga) and the intrusion of the Zhaiwa mafic dykes (~2.24 Ga), direct metallogenic association appears unlikely between them.
2. Partial melting was likely to have predominated, over crustal contamination and fractional crystallization, to control the geochemistry of the Zhaiwa mafic dykes.
3. The Zhaiwa mafic dykes were formed in an extensional setting, perhaps a back arc setting.
4. Asthenosphere upwelling may have occurred in a slab window opened during subducted slab detachment, and had heated and partially melted the overlying metasomatized mantle wedge.
5. Our work implies the existence of a 2.24 Ga back arc basin in the southern part of the TNCO and the final collision must have happened after 2.24 Ga.

Acknowledgements

Financial support from the National Natural Science Foundation of China (41372085; 41072061; 41202050) and the National Basic Research Program (No. 2012CB416602 and 2012CB416703) are gratefully acknowledged. We highly appreciate the two anonymous reviewers for the ir constructive and objective comments that significantly enhance this manuscript. Cenozoic Geoscience Editing is acknowledged for their language polishing and scientific editing services. This is contribution No. IS-2132 from GIGCAS.

References

Allegre, C.J., Minster, J.F., 1978. Quantitative models of trace element behavior in magmatic processes. Earth Planet. Sci. Lett. 38, 1–25.
Blichert-Toft, J., Albarède, F., 1997. The Lu-Hf isotope geochemistry of chondrites and the evolution of the mantle-crust system. Earth Planet. Sci. Lett. 148, 243–258.
Callegaro, S., Marzoli, A., Bertrand, H., Chiaradia, M., Reisberg, L., Meyzen, C., Bellieni, G., Weems, R.E., Merle, R., 2013. Upper and lower crust recycling in the source of CAMP basaltic dykes from southeastern North America. Earth Planet. Sci. Lett. 376, 186–199.
Castillo, P.R., Janney, P.E., Solidum, R.U., 1999. Petrology and geochemistry of Camiguin Island, southern Philippines: insights to the source of adakites and other lavas in a complex arc setting. Contrib. Mineral. Petrol. 134, 33–51.
Chen, Y.J., Fu, S.G., 1992. Gold Mineralization in West Henan, China. Seismological Press, Beijing, 234 pp. (in Chinese with English abstract).
Corfu, F., Hanchar, J.M., Hoskin, P.W., Kinny, P., 2003. Atlas of zircon textures. Rev. Mineral. Geochem. 53, 469–500.
Deng, X.H., Chen, Y.J., Santosh, M., Zhao, G.C., Yao, J.M., 2013a. Metallogeny during continental outgrowth in the Columbia supercontinent: isotopic characterization of the Zhaiwa Mo–Cu system in the North China Craton. Ore Geol. Rev. 51, 43–56.
Deng, X.H., Chen, Y.J., Santosh, M., Yao, J.M., 2013b. Genesis of the 1.76 Ga Zhaiwa Mo–Cu and its link with the Xiong'er volcanics in the North China Craton: implications for accretionary growth along the margin of the Columbia supercontinent. Precambrian Res. 227, 337–348.
DePaolo, D.J., 1988. Neodymium Isotope Geochemistry: An Introduction. Springer, New York, 181 pp.
Diwu, C.R., Sun, Y., Zhao, Y., Lai, S.C., 2014. Early Paleoproterozoic (2.45–2.20 Ga) magmatic activity during theperiod of global magmatic shutdown: implications for the crustalevolution of the southern North China Craton. Precambrian Res. 255, 627–640.
Donnelly, K.E., Goldstein, S.L., Langmuir, C.H., Spiegelman, M., 2004. Origin of enriched ocean ridge basalts and implications for mantle dynamics. Earth Planet. Sci. Lett. 226, 347–366.
Du, L.L., Yang, C.H., Guo, J.H., Wang, W., Ren, L.D., Wan, Y.S., Geng, Y.S., 2010. The age of the base of the Paleoproterozoic Hutuo Group in the Wutai area, North China Craton: SHRIMP zircon U–Pb dating of basaltic andesite. Chin. Sci. Bull. 55, 1782–1789.
Du, L.L., Yang, C.H., Ren, L.D., Song, H.X., Geng, Y.S., Wan, Y.S., 2012. The 2.2–2.1 Ga magmatic event and its tectonic implication in the Lvliang Mountains, North ChinaCraton. Acta Petrol. Sin. 28, 2751–2769 (in Chinese with English abstract).
Du, L.L., Yang, C.H., Wang, W., Ren, L.D., Wan, Y.S., Wu, J.S., Zhao, L., Song, H.X., Geng, Y.S., Hou, K.J., 2013. Paleoproterozoic rifting of the North China Craton: geochemical and zircon Hf isotopic evidence from the 2137 Ma Huangjinshan A-type granite porphyry in the Wutai area. J. Asian Earth Sci. 72, 190–202.
Fan, W.M., Wang, Y.J., Zhang, A.M., Zhang, F.F., Zhang, Y.Z., 2010. Permian arc-back-arc basin development along the Ailaoshan tectonic zone: geochemical, isotopic and geochronological evidence from the Mojiang volcanic rocks, Southwest China. Lithos 119, 553–568.
Faure, M., Trap, P., Lin, W., Monié, P., Bruguier, O., 2007. Polyorogenic evolution of the Paleoproterozoic Trans-North China Belt—new insights from the Lvliangshan-Hengshan-Wutaishan and Fuping massifs. Episodes 30, 96–107.
French, J.E., Heaman, L.M., 2010. Precise U-Pb dating of Paleoproterozoic mafic dyke swarms of the Dharwar craton, India: implications for the existence of the Neoarchean supercraton Sclavia. Precambrian Res. 183, 416–441.
Gibson, S.A., Thompson, R.N., Dickin, A.P., 2000. Ferropicrites: geochemical evidence for Fe-rich streaks in upwelling mantle plumes. Earth Planet. Sci. Lett. 174, 355–374.
Griffin, W.L., Pearson, N.J., Belousova, E., Jackson, S.E., Achterbergh, E., O'Reilly, S.Y., Shee, S.R., 2000. The Hf isotope composition of cratonic mantle: LA-MC-ICPMS analysis of zircon megacrysts in kimberlites. Geochim. Cosmochim. Acta 64, 133–147.

Guo, F., Nakamuru, E., Fan, W.M., Kobayoshi, K., Li, C.W., 2007. Generation of Paleocene adakitic andesites by magma mixing; Yanji Area, NE China. J. Petrol. 48, 661–692.
Hanski, E.J., Smolkin, V.F., 1995. Iron-LREE-enriched mantle source for early Proterozoic intraplate magmatism as exemplified by the Pechenga ferropicrites, Kola Peninsula, Russia. Lithos 34, 107–125.
Hawkesworth, C.J., Gallagher, K., Hergt, J.M., McDermott, F., 1993. Mantle and slab contribution in arc magmas. Annu. Rev. Earth Planet. Sci. 21, 175–204.
He, Y.H., Zhao, G.C., Sun, M., Xia, X.P., 2009. SHRIMP and LA-ICP-MS zircon geochronology of the Xiong'er volcanic rocks: implications for the Paleo-Mesoproterozoic evolution of the southern margin of the North China Craton. Precambrian Res. 168, 213–222.
Hellebrand, E., Snow, J.E., Hoppe, P., Hofmann, A.W., 2002. Garnet-field melting and late-stage refertilization in residual abyssal peridotites from the Central Indian Ridge. J. Petrol. 43, 2305–2338.
Herzberg, C., Asimow, P.D., 2008. Petrology of some oceanic island basalts: PRIMELT2.XLS software for primary magma calculation. Geochem. Geophys. Geosyst. 9, http://dx.doi.org/10.1029/2008GC002057.
Herzberg, C., Asimow, P.D., Arndt, N., Niu, Y., Lesher, C.M., Fitton, J.G., Cheadle, M.J., Saunders, A.D., 2007. Temperatures in ambient mantle and plumes: constraints from basalts, picrites and komatiites. Geochem. Geophys. Geosyst. 8, http://dx.doi.org/10.1029/GC001390.
Herzberg, C., Gazel, E., 2009. Petrological evidence for secular cooling in mantle plumes. Nature 458, 619–622.
Hodson, M.E., 2002. Experimental evidence for mobility of Zr and other trace elements in soils. Geochim. Cosmochim. Acta 66, 819–828.
Huang, X.L., Niu, Y.L., Xu, Y.G., Chen, L.L., Yang, Q.J., 2010. Mineralogical and geochemical constraints on the petrogenesis of post-collisional potassic and ultrapotassic rocks from western Yunnan, SW China. J. Petrol. 51, 1617–1654.
Huang, X.L., Wilde, S.A., Yang, Q.J., Zhong, J.W., 2012. Geochronology and petrogenesis of gray gneisses from the Taihua Complex at Xiong'er in the southern segment of the Trans-North China Orogen: implications for tectonic transformation in the Early Paleoproterozoic. Lithos 134–135, 236–252.
Huang, X.L., Wilde, S.A., Zhong, J.W., 2013. Episodic crustal growth in the southern segment of the Trans-North China Orogen across the Archean-Proterozoic boundary. Precambrian Res. 233, 337–357.
Jensen, L.S., 1976. A New Cation Plot for Classifying Subalkaline Volcanic Rocks, 66. Ontario Geological Survey, Miscellaneous.
Jiang, Z.S., Wang, G.D., Xiao, L.L., Diwu, C.R., Lu, J.S., Wu, C.M., 2011. Paleoproterozoic metamorphic P–T–t path and tectonic significance of the Luoning metamorphic complex at the southern terminal of the Trans-North China Orogen, Henan Province. Acta Petrol. Sin. 27 (12), 3701–3717 (in Chinese with English abstract).
Kampunzu, A.B., Tombale, A.R., Zhai, M., Bagai, Z., Majaule, T., Modisi, M.P., 2003. Major and trace element geochemistry of plutonic rocks from Francistown, NE Botswana: evidence for a Neoarchaean continental active margin in the Zimbabwe craton. Lithos 71, 431–460.
Kelley, K.A., Cottrell, E., 2012. The influence of magmatic differentiation on the oxidation state of Fe in a basaltic arc magma. Earth Planet. Sci. Lett. 329–330, 109–121.
Kinzler, R.J., 1997. Melting of mantle peridotite at pressures approaching the spinel to garnet transition: application to mid-ocean ridge basalt petrogenesis. J. Geophys. Res. Solid Earth 102, 853–874.
Köppel, V., Sommerauer, J., 1974. Trace elements and the behavior of the U-Pb system in inherited newly formed zircon grains. Contrib. Mineral. Petrol. 43, 71–82.
Kröner, A., Wilde, S.A., Li, J.H., Wang, K.Y., 2005. Age and evolution of a late Archaean to Paleoproterozoic upper to lower crustal section in the Wutaishan/Hengshan/Fuping terrain of northern China. J. Asian Earth Sci. 24, 577–595.
Kusky, T.M., Li, J.H., 2003. Paleoproterozoic tectonic evolution of the North China Craton. J. Asian Earth Sci. 22, 383–397.
Kusky, T., Li, J.H., Santosh, M., 2007. The Paleoproterozoic North Hebei Orogen: North China Craton's collisional suture with the Columbia supercontinent. Gondwana Res. 12, 4–28.
Kusky, T.M., 2011. Comparison of results of recent seismic profiles with tectonic-models of the North China Craton. J. Earth Sci. 22, 250–259.
Lana, C., Reimold, W.U., Gibson, R.L., Koeberl, C., Siegesmund, S., 2004. Nature of the Archean midcrust in the core of the Vredefort Dome, Central Kaapvaal Craton, South Africa. Geochim. Cosmochim. Acta 68, 623–642.
Le Bas, M.J., Le Maitre, R.W., Streckeisen, A., Zanettin, B., 1986. A chemical classification of volcanic rocks based on the total alkali-silica diagram. J. Petrol. 27, 745–750.
Leybourne, M.I., Van Wagoner, N., Ayres, L.D., 1999. Partial melting of a refractory subducted slab in a Paleoproterozoic island arc: implications for global chemical cycles. Geology 27, 731–734.
Li, J.H., Kusky, T., 2007. A late archean foreland fold and thrust belt in the North China Craton: implications for early collisional tectonics. Gondwana Res. 12, 47–66.
Li, N., Chen, Y.J., Deng, X.H., Yao, J.M., 2014. Fluid inclusion geochemistry and ore genesis of the Longmendian Mo deposit in the East Qinling Orogen: implication for migmatitic-hydrothermal Mo-mineralization. Ore Geol. Rev. 63, 520–531.
Li, N.B., Lou, Y., Guo, S.L., Jiang, Y.H., Zeng, L.J., Niu, H.C., 2013. Zircon U-Pb geochronology and Hf isotope geochemistry of metamorphic quartz-monzonite porphyry from Tongkuangyu area, Zhongtiao Mountain and its geological implications. Acta Petrol. Sin. 29, 2416–2424 (in Chinese with English abstract).
Li, S.Z., Zhao, G.C., 2007. Shrimp U-Pb zircon geochronology of the Liaoji granitoids: constraints on the evolution of the Paleoproterozoic Jiao-Liao-Ji belt in the Eastern Block of the North China Craton. Precambrian Res. 158, 1–16.
Lightfoot, P.C., Hawkesworth, C.J., Hergt, J., Naldrett, A.J., Gorbachev, N.S., Fedorenko, V.A., Doherty, W., 1993. Remobilization of the continental lithosphere by a mantle plume: major-, trace-element, and Sr-, Nd-, Pb-isotope evidence from picritic and tholeiitic lavas of the Noril'sk District, Siberian Trap, Russia. Contrib. Mineral. Petrol. 114, 171–188.
Liu, C.H., Zhao, G.C., Liu, F.L., Shi, J.R., 2014a. Geochronological and geochemical constraints on the Lüliang Group in the Lüliang Complex: implications for the tectonic evolution of the Trans-North China Orogen. Lithos 198, 298–315.
Liu, C.H., Zhao, G.C., Liu, F.L., Shi, J.R., 2014b. 2.2 Ga magnesian andesites, Nb-enriched basalt-andesites, and adakitic rocks in the Lüliang Complex: evidence for early Paleoproterozoic subduction in the North China Craton. Lithos 208, 104–117.
Liu, D.Y., Nutman, A.P., Compston, W., Wu, J.S., Shen, Q.H., 1992. Remnants of 3800 Ma crust in the Chinese Part of the Sino-Korean craton. Geology 20, 339–342.
Liu, S.W., Zhang, J., Li, Q.G., Zhang, L.F., Wang, W., Yang, P.T., 2012. Geochemistry and U-Pb zircon ages of metamorphic volcanic rocks of the Paleoproterozoic Lüliang Complex and constraints on the evolution of the Trans-North China Orogen, North China Craton. Precambrian Res. 222–223, 173–190.
Liu, Y.S., Gao, S., Hu, Z.C., Gao, C.G., Zong, K.Q., Wang, D.B., 2010. Continental and oceanic crust recycling-induced melt–peridotite interactions in the Trans-North China Orogen: U-Pb dating, Hf isotopes and trace elements in zircon grains from mantle xenoliths. J. Petrol. 51, 537–571.
Ludwig, K., 2003. User's manual for ISOPLOT 3.00: a geochronological toolkit for Microsoft Excel, Special Publication No. 4. Berkeley Geochronology Center 71.
Ma, L., Wang, Q., Wyman, D.A., Jiang, Z.Q., Yang, J.H., Li, Q.L., Gou, G.N., Guo, H.F., 2013. Late Cretaceous crustal growth in the Gangdese area, southern Tibet: petrological and Sr-Nd-Hf-O isotopic evidence from Zhengga diorite-gabbro. Chem. Geol. 349–350, 54–70.
Martin, H., Smithies, R.H., Rapp, R., Moyen, J., Champion, D., 2005. An overview of adakite, tonalite-trondhjemite-granodiorite (TTG), and sanukitoid: relationships and some implications for crustal evolution. Lithos 79, 1–24.
McKenzie, D., O'Nions, R.K., 1991. Partial melt distribution from inversion of rare earth element concentrations. J. Petrol. 32, 1021–1091.
Menzies, M., Chazot, G., 1995. Fluid processes in diamond to spinel facies shallow mantle. J. Geodyn. 20, 387–415.
Middlemost, E.A., 1994. Naming materials in the magma/igneous rock system. Earth Sci. Rev. 37, 215–224.
Pearce, J.A., Stern, R.J., 2006. Origin of back-arc basin magmas: trace element and isotope perspectives. Geophys. Monogr., 63–86.
Peng, P., Zhai, M.G., Zhang, H.F., Guo, J.H., 2005. Geochronological constraints on the Paleoproterozoic evolution of the North China Craton: SHRIMP zircon ages of different types of Mafic Dikes. Int. Geol. Rev. 47, 492–508.
Peng, P., Guo, J.H., Zhai, M.G., Windley, B.F., Li, T.S., Liu, F., 2012. Genesis of the hengling magmatic belt in the North China Craton: implications for Paleoproterozoic tectonics. Lithos 148, 27–44.
Plank, T., 2005. Constraints from thorium/lanthanum on sediment recycling at subduction zones and the evolution of the continents. J. Petrol. 46, 921–944.
Polat, A., Hofmann, A.W., Rosing, M.T., 2002. Boninite-like volcanic rocks in the 3.7–3.8 Ga Isua greenstone belt, West Greenland: geochemical evidence for intra-oceanic subduction zone processes in the early Earth. Chem. Geol. 184, 231–254.
Rogers, N., Macdonald, R., Fitton, J.G., George, R., Smith, M., Barreiro, B., 2000. Two mantle plumes beneath the East African rift system: Sr, Nd and Pb isotope evidence from Kenya Rift basalts. Earth Planet. Sci. Lett. 176, 387–400.
Rudnick, R.L., 1995. Making continental crust. Nature 378, 571–577.
Rudnick, R.L., Gao, S., 2003. Composition of the continental crust. Treatise Geochem. 3, 1–64.
Rudnick, R.L., Gao, S., Ling, W.L., Liu, Y.S., McDonough, W.F., 2004. Petrology and geochemistry of spinel peridotite xenoliths from Hannuoba and Qixia, North China Craton. Lithos 77, 609–637.
Shaw, D.M., 1970. Trace element fractionation during anatexis. Geochim. Cosmochim. Acta 34, 237–243.
Shervais, J.W., 1982. Ti–V plots and the petrogenesis of modern and ophiolitic lavas. Earth Planet. Sci. Lett. 59, 101–118.
Söderlund, U., Patchett, P.J., Vervoort, J.D., Isachsen, C.E., 2004. The 176 Lu decay constant determined by Lu-Hf and U-Pb isotope systematics of Precambrian mafic intrusions. Earth Planet. Sci. Lett. 219, 311–324.
Sun, S.S., McDonough, W.F., 1989. Chemical and isotopic systematics of oceanic basalts: implications for mantle composition and processes. In: Sunders, A.D., Norry, M.J. (Eds.), Magmatism in the Ocean Basins, vol. 42. Special Publications, London, pp. 313–345.
Takahahshi, E., Nakajima, K., Wright, T.L., 1998. Origin of the Columbia River basalts: melting model of a heterogeneous plume head. Earth Planet. Sci. Lett. 162, 63–80.
Trap, P., Faure, M., Lin, W., Monié, P., 2007. Late Paleoproterozoic (1900–1800 Ma) nappe stacking and polyphase deformation in the Hengshan–Wutaishan area: implications for the understanding of the Trans-North-China Belt, North China Craton. Precambrian Res. 156, 85–106.
Trap, P., Faure, M., Lin, W., Breton, N.L., Monie, P., 2012. The Paleoproterozoic evolution of the Trans-North China Orogen: toward a synthetic tectonic model. Precambrian Res. 222–223, 191–211.
Vermeesch, P., 2006. Tectonic discrimination diagrams revisited. Geochem. Geophys. Geosyst. 7, 466–480.
Wang, H., Wu, Y.B., Qin, Z.W., Zhu, L.Q., Liu, Q., Liu, X.C., Gao, S., Wijbrans, J.R., Zhou, L., Gong, H.J., 2013. Age and geochemistry of Silurian gabbroic rocks in the Tongbai orogen, central China: implications for the geodynamic evolution of the North Qinling arc-back-arc system. Lithos 179, 1–15.

Wang, X., Zhu, W.B., Ge, R.F., Luo, M., Zhu, X.Q., Zhang, Q.L., Wang, L.S., Ren, X.M., 2014. Two episodes of Paleoproterozoic metamorphosed mafic dykes in the Lvliang Complex: implications for the evolution of the Trans-North China Orogen. Precambrian Res. 243, 133–148.
Wang, C.Y., Campbell, I.H., Allen, C.M., Williams, I.S., Eggins, S.M., 2009. Rate of growth of the preserved North American continental crust: evidence from Hf and O isotopes in Mississippi detrital zircon grains. Geochim. Cosmochim. Acta 73, 712–728.
Wang, Z.H., Wilde, S.A., Wan, J.L., 2010. Tectonic setting and significance of 2.3–2.1 Ga magmatic events in the Trans-North China Orogen: new constraints from the Yanmenguan mafic–ultramafic intrusion in the Hengshan-Wutai-Fuping area. Precambrian Res. 178, 27–42.
Wei, X., Xu, Y.G., Feng, Y.X., Zhao, J.X., 2014. Plume-lithosphere interaction in the generation of the Tarim large igneous province, NW China: geochronological and geochemical constraints. Am. J. Sci. 314, 314–356.
Wiedenbeck, M., Alle, P., Corfu, F., Griffin, W.L., Meier, M., Oberli, F., Vonquadt, A., Roddick, J.C., Speigel, W., 1995. 3 natural zircon standards for U-Th-Pb, Lu-Hf, trace-element and REE analyses. Geostand. Newslett. 19, 1–23.
Winchester, J.A., Floyd, P.A., 1977. Geochemical discrimination of different magma series and their differentiation products using immobile elements. Chem. Geol. 20, 325–343.
Wood, B.J., Blundy, J.D., 1997. A predictive model for rare earth element partitioning between clinopyroxene and anhydrous silicate melt. Contrib. Mineral. Petrol. 129, 166–181.
Woodhead, J.D., Hergt, J.M., Davidson, J.P., Eggins, S.M., 2001. Hafnium isotope evidence for 'conservative' element mobility during subduction zone processes. Earth Planet. Sci. Lett. 192, 331–346.
Wu, C.Z., Santosh, M., Chen, Y.J., Samson, I.M., Lei, R.X., Dong, L.H., Qu, X., Gu, L.X., 2014. Geochronology and geochemistry of Early Mesoproterozoic meta-diabase sills from Quruqtagh in the northeastern Tarim Craton: implications for breakup of the Columbia supercontinent. Precambrian Res. 241, 29–43.
Wu, F.Y., Li, X.H., Zheng, Y.F., Gao, S., 2007. Lu-Hf isotopic systematics and their applications in petrology. Acta Petrol. Sin. 23, 185–220 (in Chinese with English Abstract).
Wu, Y.B., Zheng, Y.F., 2004. Genesis of Zircon and its constrains on interpretation of U-Pb age. Chin. Sci. Bull. 49 (16), 1589–1604.
Xu, Y.G., Lan, J.B., Yang, Q.J., Huang, X.L., Qiu, H.N., 2008. Eocene break-off of the Neo-Tethyan slab as inferred from intraplate-type mafic dykes in the Gaoligong orogenic belt, eastern Tibet. Chem. Geol. 255, 439–453.
Yang, C.H., Du, L.L., Ren, L.D., Song, H.X., Wan, Y.S., Xie, H.Q., Liu, Z.X., 2011. The age and petrogenesis of the Xuting granite in the Zanhuang Complex, Hebei Province: constraints on the structural evolution of the Trans-North China Orogen, North China Craton. Acta Petrol. Sin. 27, 1003–1016 (in Chinese with English abstract).
Yu, X.Q., Liu, J.L., Li, C.L., Chen, S.Q., Dai, Y.P., 2013. Zircon U-Pb dating and Hf isotope analysis on the Taihua Complex: constraints on the formation and evolution of the Trans-North China Orogen. Precambrian Res. 230, 31–44.
Yuan, H.L., Gao, S., Liu, X.M., Li, H.M., Günther, D., Wu, F.Y., 2004. Accurate U-Pb age and trace element determinations of zircon by laser ablation-inductively coupled plasma-mass spectrometry. Geostand. Geoanal. Res. 28, 353–370.
Zhai, M.G., Liu, W.J., 2003. Palaeoproterozoic tectonic history of the North China craton: a review. Precambrian Res. 122, 183–199.
Zhang, G.W., Bai, Y.B., Song, Y., Guo, A.L., Zhou, D.W., Li, T.H., 1985. Composition and evolution of the Archean crust in central Henan, China. Precambrian Res. 27, 7–35.
Zhang, Y.Z., Wang, Y.J., Geng, H.Y., Zhang, Y.H., Fan, W.M., Zhong, H., 2013. Early Neoproterozoic (~850 Ma) back-arc basin in the Central Jiangnan Orogen (Eastern South China): geochronological and petrogenetic constraints from meta-basalts. Precambrian Res. 231, 325–342.
Zhang, Z.Q., Li, S.M., 1998. Sm–Nd, Rb–Sr age and its geological significance of Archean Taihua Group in Xiong'ershan, western Henan province. In: Chen, Y.Q. (Ed.), Contributions of Early Precambrian Geology in North China Craton. Geological Publishing House, Beijing, pp. 123–132.
Zhao, G.C., Wilde, S.A., Cawood, P.A., Lu, L.Z., 1998. Thermal evolution of the Archaean basement rocks from the eastern part of the North China Craton and its bearing on tectonic setting. Int. Geol. Rev. 40, 706–721.
Zhao, G.C., Wilde, S.A., Cawood, P.A., Sun, M., 2001. Archean blocks and their boundaries in the North China Craton: lithological, geochemical, structural and T–T path constraints and tectonic evolution. Precambrian Res. 107, 45–73.
Zhao, G.C., Sun, M., Wilde, S.A., 2003. Major tectonic units of the North China Craton and their Paleoproterozoic assembly. Sci. China Ser. D: Earth Sci. 46, 23–38.
Zhao, G.C., Sun, M., Wilde, S.A., Li, S.Z., 2005. Late Achean to Paleoproterozoic evolution of the North China Craton: key issues revisited. Precambrian Res. 136, 177–202.
Zhao, G.C., Liu, S.W., Sun, M., Li, S.Z., Simon, W., Xia, X.P., Zhang, J., He, Y.H., 2007. What happened in the Trans-North China Orogen in the period 2560–1850 Ma? Acta Geol. Sin. Engl. Ed. 80, 790–806.
Zhao, G.C., He, Y.H., Sun, M., 2009. The Xiong'er volcanic belt at the southern margin of the North China Craton: petrographic and geochemical evidence for its outboard position in the Paleo-Mesoproterozoic Columbia Supercontinent. Gondwana Res. 16, 170–181.
Zhao, R.F., Guo, J.H., Peng, P., Liu, F., 2011. 2.1 Ga crustal remelting event in Hengshan Complex: evidence from zircon U-Pb dating and Hf-Nd isotopic study on potassic granites. Acta Petrol. Sin. 27, 1607–1623 (in Chinese with English abstract).
Zhou, Y.Y., Zhao, T.P., Zhai, M.G., Gao, J.F., Lan, Z.W., Sun, Q.Y., 2015. Petrogenesis of the 2.1 Ga Lushan garnet-bearing quartz monzonite on the southern margin of the North China Craton and its tectonic implications. Precambrian Res. 256, 241–255.